AD-A181 908 OPTICAL PHYSICS STUDY OF LASER INTERACTIONS WITH SOLIDS 1/1
FOR ULTRA-TRACE M (U) ATOM SCIENCES INC OAK RIDGE TN
N THONNARD ET AL 24 APR 87 AFOSR-TR-87-0706
UNCLASSIFIED F49620-86-C-0073 F/G 7/1 NL

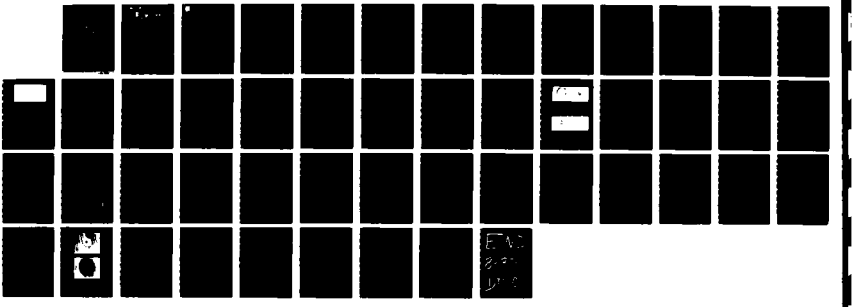

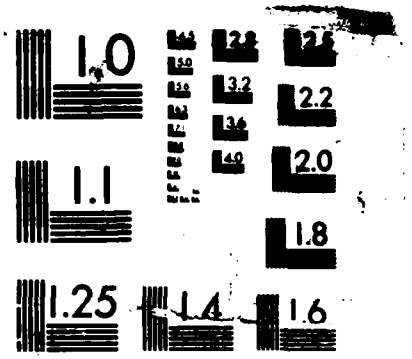

MICROCOPY RESOLUTION TEST CHART

Unclassified
SECURITY CLASSIFICATION OF THIS PAGE

DTIC FILE COPY

REPORT DOCUMENTATION

1a. REPORT SECURITY CLASSIFICATION
Unclassified

AD-A181 908

2a. SECURITY CLASSIFICATION AUTHORITY

2b. DECLASSIFICATION / DOWNGRADING SCHEDULE

Approved for public release; distribution unlimited

4. PERFORMING ORGANIZATION REPORT NUMBER(S)

5. MONITORING ORGANIZATION REPORT NUMBER(S)
AFOSR-TR- 87-0706

6a. NAME OF PERFORMING ORGANIZATION	6b. OFFICE SYMBOL (If applicable)	7a. NAME OF MONITORING ORGANIZATION
Atom Sciences, Inc.	G0138	AFOSR

6c. ADDRESS (City, State, and ZIP Code)	7b. ADDRESS (City, State, and ZIP Code)
114 Ridgeway Center Oak Ridge, TN 37830	Bldg 410 Bolling AFB, DC 20332-6448

8a. NAME OF FUNDING / SPONSORING ORGANIZATION	8b. OFFICE SYMBOL (If applicable)	9. PROCUREMENT INSTRUMENT IDENTIFICATION NUMBER
AFOSR	NP	F49620-86-C-0073

8c. ADDRESS (City, State, and ZIP Code)	10. SOURCE OF FUNDING NUMBERS			
	PROGRAM ELEMENT NO.	PROJECT NO.	TASK NO.	WORK UNIT ACCESSION NO.
Bldg, 410 Bolling AFB, DC 20332-6448	6110 2F	2301	A1	

11. TITLE (Include Security Classification)
Optical Physics Study of Laser Interactions with Solids for Ultra-Trace Materials Analysis Using RIS

12. PERSONAL AUTHOR(S)
Thonnard, Norbert and Beekman, Daniel W.

13a. TYPE OF REPORT	13b. TIME COVERED	14. DATE OF REPORT (Year, Month, Day)	15. PAGE COUNT
Final Technical	FROM 7/1/86 TO 2/28/87	1987 April 24	44

16. SUPPLEMENTARY NOTATION

17. COSATI CODES			18. SUBJECT TERMS (Continue on reverse if necessary and identify by block number)
FIELD	GROUP	SUB-GROUP	
			Element Analysis; Ultra-Trace, Laser Ablation; Resonance Ionization; Semiconductor Impurities; Materials Characterization; Parts per Trillion, Sensitivity; Selectivity; Interference Reduction; Quantitation

19. ABSTRACT (Continue on reverse if necessary and identify by block number)

The feasibility of a new element analysis technique having sensitivity in the sub-part per billion range was investigated. The method combines pulsed laser volatilization of a representative fraction of the sample with selective and efficient ionization of the element of interest by utilizing lasers tuned to specific transitions of the selected element. Tests on silicon and steel substrates determined cratering characteristics at incident power densities ranging from 10^7 to 2×10^{11} W/cm^{-2}. The quantity of material volatilized was proportional to the number of laser shots. A simple time-of-flight mass spectrometer was assembled, which together with the volatilization laser and resonance ionization laser was used to demonstrate the technique by analyzing 0.48 to 58 ppm Ga in Si samples. Sensitivity of 15 ppb was demonstrated, while the resonance ionization element selectivity was $>10^8$. Guidelines were established for development of a prototype system with a 5 μm analysis spot, a resonance ionization laser system for 80 elements, and a time-of-flight mass spectrometer with ablated ion rejection, thereby achieving sensitivity at the part in 10^{12} range.

20. DISTRIBUTION / AVAILABILITY OF ABSTRACT	21. ABSTRACT SECURITY CLASSIFICATION
☑ UNCLASSIFIED/UNLIMITED ☑ SAME AS RPT. ☐ DTIC USERS	Unclassified

22a. NAME OF RESPONSIBLE INDIVIDUAL	22b. TELEPHONE (Include Area Code)	22c. OFFICE SYMBOL
Dr. Howard R. Schlossberg	202-767-4906	NP

DD FORM 1473, 84 MAR

83 APR edition may be used until exhausted.
All other editions are obsolete.

SECURITY CLASSIFICATION OF THIS PAGE
Unclassified

ATOM SCIENCES, INCORPORATED
114 Ridgeway Center
Oak Ridge, Tennessee 37830 (615) 483-1113

OPTICAL PHYSICS STUDY OF LASER INTERACTIONS WITH SOLIDS FOR ULTRA-TRACE MATERIALS ANALYSIS USING RIS

SBIR PHASE I FINAL REPORT

Contract Number: F49620-86-C-0073
July 1, 1986 - February 28, 1987

Prepared for

Dr. Howard R. Schlossberg
AFOSR
Directorate of Physical and Geophysical Sciences
Building 410
Bolling AFB, DC 20332-6448

by

Atom Sciences, Inc.
114 Ridgeway Center
Oak Ridge, Tennessee 37830

Dr. Norbert Thonnard, Principal Investigator
Dr. Daniel W. Beekman, Investigator

April 24, 1987

Approved for public release; distribution unlimited.

TABLE OF CONTENTS

Accesion For	
NTIS CRA&I	☑
DTIC TAB	☐
Unannounced	☐
Justification	
By	
Distribution /	
Availability Codes	
Dist	Avail and / or Special
A-1	

LIST OF FIGURES

SUMMARY

There is a critical need in the fields of materials science and semiconductor research and development to determine the trace element composition at the parts per million (ppm), ppb or even the ppt level. It is also frequently necessary to make these determinations as a function of position and depth. During this Phase I research and development program, the feasibility of combining laser ablation, an efficient, spatially resolved sample volatilization technique with Resonance Ionization Spectroscopy (RIS), an ultra-sensitive and selective element analysis technique has been demonstrated.

After characterization of the Nd:YAG laser system used, ablation tests on silicon and steel substrates showed that at power densities of $\sim 2 \times 10^{11}$ W cm^{-2}, craters 5 to 10 times larger than the laser beam were generated, while at power densities of 10^8 to 10^9 W cm^{-2}, the affected area was equivalent to the laser beam diameter. Analysis spots as small as 30 μm were generated, which with appropriate optics could be reduced to ~ 2 μm. The depth of craters generated and material volatilized was proportional to the number of laser shots. At the power densities used for sample analysis, $\sim 10^7$ W cm^{-2}, measurable marks were not apparent on the samples.

A simple time-of-flight mass spectrometer was assembled and used with the laser ablation system and an available RIS laser system to demonstrate the sensitivity and selectivity of the technique. Silicon samples with known concentrations of gallium (0.48 to 58 ppm) as well as steel reference materials with certified aluminum concentrations (7 ppm to 2,400 ppm) were analyzed with the system. Good correlation of observed RIS gallium signal with concentration was obtained for the silicon samples. Due to the high efficiency of the RIS process, low ablation power densities were necessary, therefore few background ions were created during the ablation process. By appropriate adjustment of the ablation and RIS time delay, potential interferences could be eliminated. Averaging the mass spectra from only 500 laser shots (50 seconds with this system) resulted in a detection limit of ~ 15 ppb. The selectivity of the RIS process was shown to be greater than one part in 10^8 by comparing the ^{28}Si signal with the ^{69}Ga signal in the TOF mass spectrum. The potential of sensitivity in the part in 10^{12} range seems realistic.

General guidelines for development of a prototype solids analysis system during Phase II were given. The proposed system would have an analysis spot size of 5 μm, an RIS system capable of analyzing ~ 80 elements with the same laser system, and a TOF mass spectrometer system capable of rejecting ablated ions, thereby achieving sensitivity at the part in 10^{12} range.

I. INTRODUCTION

Determination of the elemental composition of solid materials is a fundamental need in the field of materials science. This is especially true in semiconductor research and development projects, where specific elements (dopants) need to be at the parts per million (ppm) level, while other trace elements (impurities) may seriously alter or degrade device performance even if they are in the low ppb or ppt range. In many instances, not only is bulk material analysis of interest, but also the change in composition with depth and position across the surface. Therefore, an ultra-sensitive element analysis technique that can probe a solid material directly, having depth resolution in the sub-micrometer, and lateral resolution in the few micrometer range, would be extremely valuable.

Mass spectrometry is one of the most frequently used methods of trace element analysis, of which thermal vaporization and ionization is presently perhaps the most sensitive and accurate approach. The vaporization and ionization processes are well understood, allowing predictable and accurate results. Unfortunately, for most substances the ion yield is a very small fraction of the material evolved, limiting the ultimately achievable sensitivity. In addition, this is not a direct method, requiring careful chemical separation and loading of the residual material on a filament, introducing several potential routes for contamination. Positional information can only be obtained indirectly.

Secondary Ion Mass Spectrometry (SIMS) has become an established surface analysis technique and is frequently used to measure impurities in semiconductor materials. In the SIMS technique, material is removed from a surface by sputtering with an intense ion beam. By controlling the ion beam energy, size and intensity, good depth and lateral resolution can be achieved, but due to ion beam density limitations, the achievable sensitivity suffers at high lateral resolutions. Most of the material leaving the surface is in the form of neutral atoms or molecules, with a small fraction being ionized. The yield of secondary ions is highly dependent on the type of secondary ion, the host matrix, and the surface

condition. A mass spectrometer is used for identification of the ionized species and is subject to interferences from isobaric effects and molecular ionization.

Due to the ease with which coherent radiation from lasers can be focused and time modulated, it is possible to control and deliver energy to solid surfaces at power densities that are adjustable over an extremely large range. It was recognized early (1) that a pulsed laser could potentially be a very interesting vapor source for mass spectrometric solid material analysis, enabling direct analysis with the possibility of good depth and lateral resolution. Over the power density range frequently used in various laser analysis techniques (2), 10^6 to 10^{11} W cm^{-2}, the effects to the solid sample change dramatically from removal of adsorbed elements or molecules, to violent conversion of the surface and underlying material to a plasma, and frequently even to the point of ejecting solid and liquid particles. At power levels below 10^8 W cm^{-2}, the ratio of ions to neutrals is very low, whereas above $5x10^9$ W cm^{-2} ionization approaches 100% (2). At high power densities, due to the plasma that is formed, the large ion energy spread degrades mass spectrometer performance, whereas at lower power densities, sensitivity is low due to the poor ionization efficiency.

From the above discussions, it is apparent that a major limitation in most of the mass spectrometry techniques is the ionization process. It is usually of very low efficiency and variable, due to dependence on surface and matrix effects, or so violent and indiscriminant (as in laser ablation plasma formation) that mass analysis and quantification becomes difficult.

II. BACKGROUND

There is a critical need for new ultra-trace analytical techniques applicable in the fields of materials research and semiconductor research. Desirable properties include considerably increased sensitivity, better quantitation, freedom from molecular and isobaric interferences, and good lateral and depth resolution. Resonance Ionization Spectroscopy (RIS) has the potential of solving some of the limitations of the analytical techniques mentioned previously.

RIS, a new technique for ultra-trace element analysis, was first developed at Oak Ridge National Laboratory (3,4) by G. S. Hurst and co-workers. Subsequently the RIS concept was generalized and shown to be potentially feasible with present-day laser techniques for all elements of the periodic table except He and Ne (5). This ionization method is extremely selective as laser wavelengths can be chosen to promote an electron from the ground state through several excited states that are unique to that particular element, and then to the ionization continuum. The power available from modern pulsed dye lasers is sufficient to saturate most atomic transitions in a reasonable volume of space, making this method also extremely sensitive, as all selected atoms in that volume will be ionized. Once ionized, the selected atoms can be counted with conventional charged particle detectors. Unlike SIMS, the ionization efficiency of RIS should be constant for most elements.

Atom Sciences, Inc., combining the ultra-sensitivity and selectivity of RIS with sputtering, has provided a solid analysis technique (6) called Sputter Initiated Resonance Ionization Spectroscopy (SIRIS), (patented). A pulsed ion beam is used to remove (sputter) a representative sample of atoms from the solid surface. The expanding cloud (mostly neutral atoms with a few secondary ions which are suppressed) is probed by the RIS laser beams that ionize all the atoms of the selected element within the beams. The technique eliminates interferences which are generated by non-resonant ionization processes such as thermal ionization and electron bombardment. SIRIS has demonstrated measurements of impurities in both silicon and

gallium arsenide, matrices of interest in semiconductor research and development, and has demonstrated detection limits as low as 2 ppb (7) with the present instrument at Atom Sciences.

Even though the SIRIS technique is becoming an extremely valuable surface analysis method having broad applicability, there are some physical limitations in the atomization process, i.e., the "sputter initiated" part of SIRIS, that may become a problem at the ppt analysis level. Firstly, as the ion beam actually penetrates the sample, any impurities in the ion beam will be buried into the sample, including contaminants on the sample surface. Secondly, 50 mA cm^{-2} appears to be the current density limit achievable at the desired ion bombardment energies. Therefore, if one desires analysis in a 10 micrometer spot, using the 50 mA cm^{-2} ion density limit, only 40 nA of ion current would be available for sputtering. Therefore, the 25% measurement limit (20 counts) in 10 minutes analysis time using typical SIRIS parameters (30 Hz repetition rate, 10^{-6} sec pulse width, detection of 10% of sputtered material) would be $\sim$ 40 ppb. And finally, analysis of insulating samples is difficult in either SIMS or SIRIS. Because of the charge in the incoming ion beam and the secondary electrons produced in the ion bombardment process, insulating samples become charged to high potentials, modifying the ion extraction optics in a random fashion and frequently producing inconsistent results. With a photon beam this problem may not exist, unless photo-electron emission is severe. Because of the extreme element selectivity possible with RIS, and as only an extremely small fraction of the RIS photons are absorbed, the sensitivity limit is directly proportional to the neutral atom density in the laser beam. Combining the high atomization rate which occurs in laser ablation with the high element - specificity and ionization efficiency of RIS should provide a very powerful tool for ultra-trace element analysis.

The combination of laser ablation with RIS for ultra-trace solids analysis was first reported by Beekman, et al. (8). Mayo and collaborators (9) at the National Bureau of Standards ablated 5×10^{14} atoms from a silicon sample followed by ionization with lasers tuned to the sodium resonance inside of a proportional counter. They detected an

estimated sodium concentration of 5×10^{11} Na cm^{-3}, but had difficulty quantifying the measurements. Subsequently, Beekman and Callcott combined laser ablation with RIS and time-of-flight mass spectrometry for analysis of samarium in solid samples (10).

The solid materials analysis possibilities using laser ablation for atomization and RIS for ionization are very exciting. By separating atomization from ionization, it should be possible to optimize each process for the analytical requirements. With the high ionization efficiency and selectivity of the RIS process, a reasonable fraction of the atoms from the selected element in the ablated neutral atom plume could be ionized and detected without interference from the major constituents of the sample. Considering that neutral atom densities as high as 10^{20} cm^{-3} have been observed for thorium metal heated with 10^{7} W cm^{-2}, 10 μsec laser pulses (11) and that selectivity $>10^{11}$ has been observed in the RIS of rhenium atoms (12), in principle it should be possible to achieve a sensitivity approaching 1 part in 10^{15}.

III. PROJECT OBJECTIVES

The overall objective of this Phase I effort was to demonstrate the feasibility of laser ablation or evaporation as a source of neutral atoms for ultra-sensitive trace element analysis in solids using RIS. Existing facilities were to be modified to demonstrate feasibility and recommendations made for pursuit during Phase II. The following specific tasks were identified:

1. Modify and characterize Quantel YG-480 Nd:YAG laser and determine its suitability for ablation studies. Measure temporal and spatial pulse shape as a function of Q-switch delay; determine energy-pulse width relationship at 1064 and 532 nm.

2. Measure ablation crater shape as a function of pulse width, power density and wavelength in steel and silicon. Determine reproducibility of cratering, differences between steel and silicon, and controllability with multiple shots at one location.

3. Modify existing RIS-TOF system for ablation studies.

4. Measure the RIS and non-resonant TOF spectrum under differing ablation conditions in steel and silicon samples. Determine the RIS signal vs. concentration relationship for aluminum in steel and gallium in silicon.

5. Assess results of tasks 1., 2. and 4. and determine if present laser is suitable as an ablation source. Make recommendations for research directions and equipment needs during Phase II.

IV. STATUS OF RESEARCH EFFORT

1. Ablation Laser Characterization

In a pulsed Nd:YAG laser, flashlamps are used to supply energy to the laser rod while an electro-optic Q-switch prevents lasing until the stored energy in the rod is maximum. When the Q-switch is triggered, the stored energy is released in an intense laser pulse. The laser pulse width and energy were measured as functions of flashlamp energy and the Q-switch delay time. These data were then used in an investigation of the ablation process as a function of laser parameters.

The laser pulse shape was measured using a fast photodiode and a LeCroy 9400 digital oscilloscope in the interleaved sampling mode yielding 80 psec time resolution. Fluctuations in laser pulse energy from shot to shot appear as noise in the interleaved data, but averaging of several such traces gives a good indication of the typical pulse shape. Using the normal operating parameters for the laser (flashlamp voltage = 1500 V, Q-switch delay = 190 μsec), the oscilloscope trace shown in Figure 1 was obtained by averaging ten interleaved traces of the highly attenuated infrared (IR) laser beam monitored with the photodiode. The mode structure of the laser pulse and the noise at the baseline are reproducible, both for individual interleaved traces and for separate averages. Since the mode structure can affect the measured full width half maximum (FWHM) and the mode structure changes with flashlamp voltage and Q-switch delay, we define the laser pulse width as the FWHM of a smooth curve approximating the actual laser pulse, which has been done by eye for the peak widths reported here.

The total energy per pulse can be measured with a calorimeter or inferred by integrating the photodiode signal of Figure 1, which is a measure of instantaneous power vs. time. In Figure 2, the peak power, measured with the photodiode, and the total energy per pulse, measured by the calorimeter, are plotted together, again for the IR laser beam with flashlamp voltage at 1500 V.

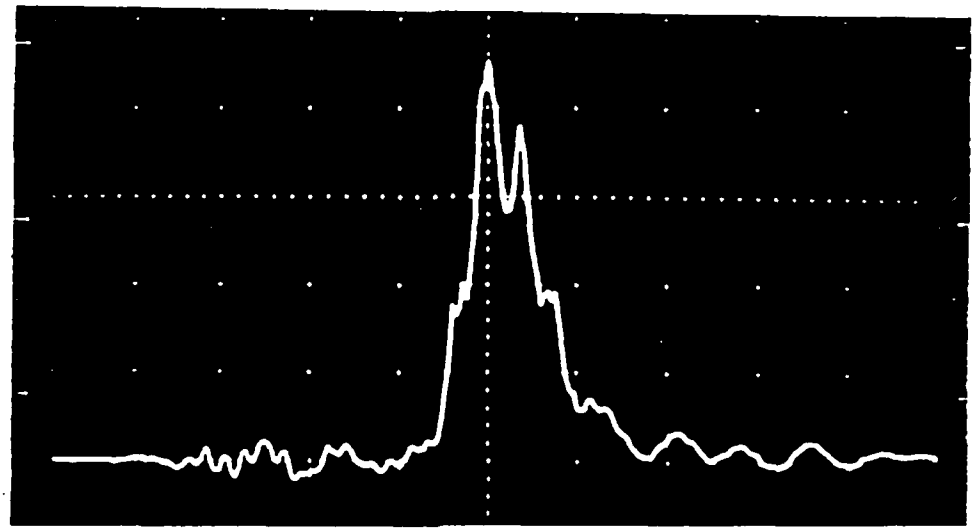

Figure 1. Temporal laser pulse shape at nominal operating conditions. The time base is 10 nsec/division; the vertical scale, arbitrary. The shape of the peak is reproducible, an indication that the observed signal is due to the mode structure of the pulse.

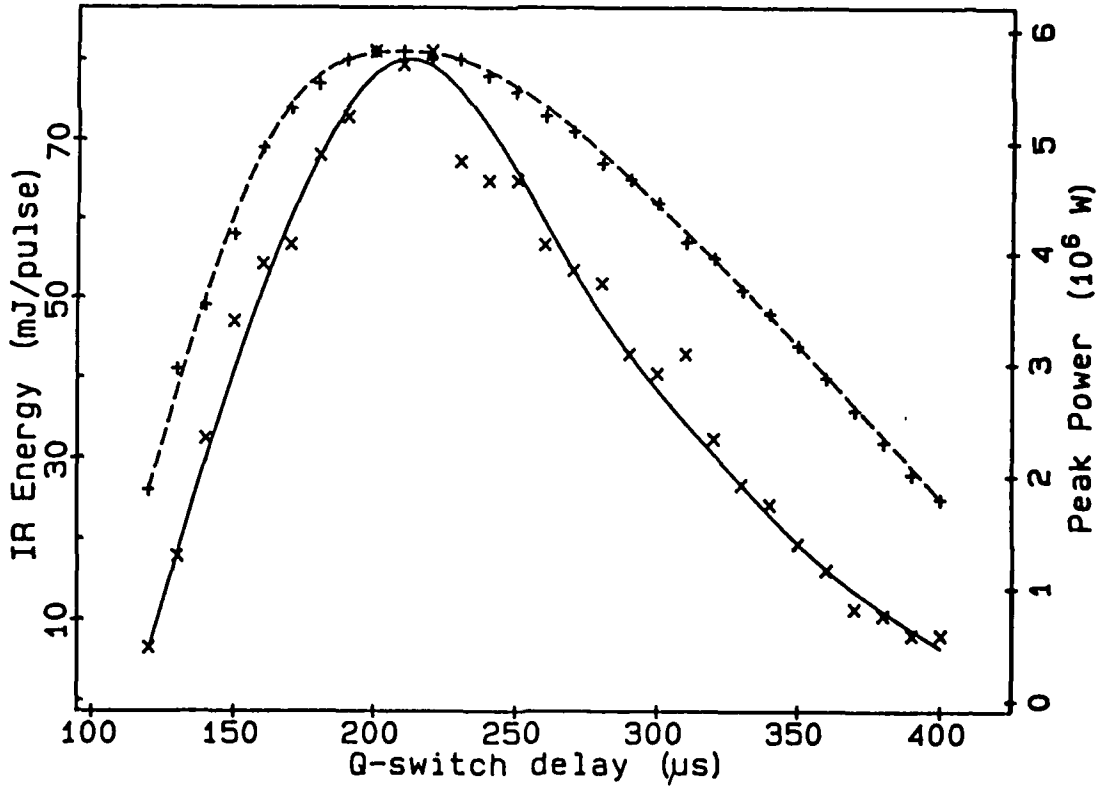

Figure 2. Peak power and pulse energy as a function of Q-switch delay at flashlamp voltage of 1500 V.

For a Q-switch delay of about 200 μsec both the energy and peak power are maximized. At shorter and longer delay times, the peak power decreases faster than the pulse energy, due to the longer pulse duration.

The normalized peak power for both the IR fundamental wavelength and the second harmonic wavelength at 532 nm (green) as a function of Q-switch delay time at a flashlamp voltage 1500 V is shown in Figure 3. Note that both wavelengths reach maximum peak power at about the same Q-switch delay, while the conversion efficiency decreases slightly for other delay times. The variation of peak power with flashlamp voltage is shown in Figure 4 for both IR and green wavelengths using a Q-switch delay of 190 μsec. Here the peak power at both wavelengths and the conversion efficiency are all maximum at the maximum flashlamp voltage. For low flashlamp voltages (<1400 V) and also for both very short (<120 μsec) and very long (>400 μsec) Q-switch delays, the peak power and energy were not only low, but also very erratic. Hence, data was not acquired at the more extreme values, limiting the range of pulse widths obtainable in practice.

The peak width as a function of Q-switch delay is shown in Figure 5, again at both wavelengths and 1500 V on the flashlamps. The dependence is essentially the same at both wavelengths, with the green pulse slightly shorter. Note that at short and long Q-switch delays, the pulse width is only three to four times the minimum pulse width. Finally, the dependence of pulse width on flashlamp voltage is shown in Figure 6, for a 190 μsec Q-switch delay. The shortest pulse width occurs at the highest flashlamp voltage, while the longest pulse widths are only three times the shortest, with the green pulse slightly shorter than the IR pulse.

The other laser beam parameter of importance is the spatial energy distribution, or beam profile. This was determined for a range of Q-switch delay times and flashlamp voltages by taking burn patterns on photosensitive paper. The burn patterns crudely confirmed the variation of total beam energy with Q-switch delay and flashlamp voltage, but as they were mostly highly saturated, did not reveal significant variations in energy distribution for the parameter ranges used. A few spot checks of the beam profile were made by using the laser to anneal a piece of lapped

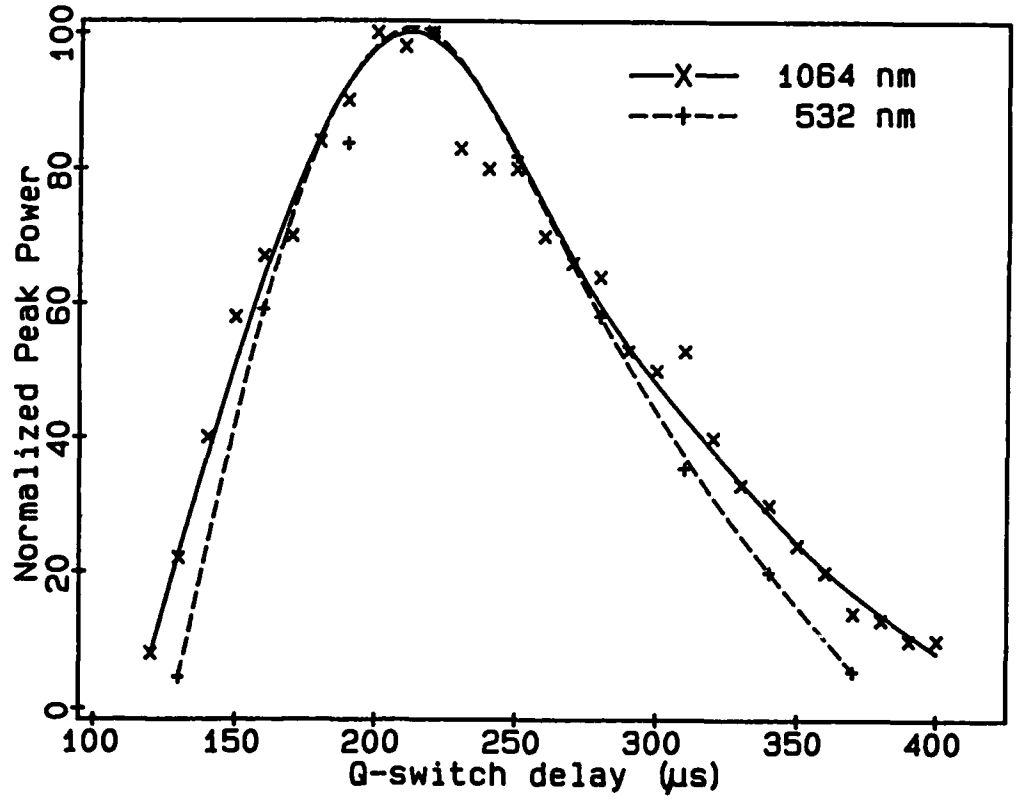

Figure 3. IR and green peak power as a function of Q-switch delay.

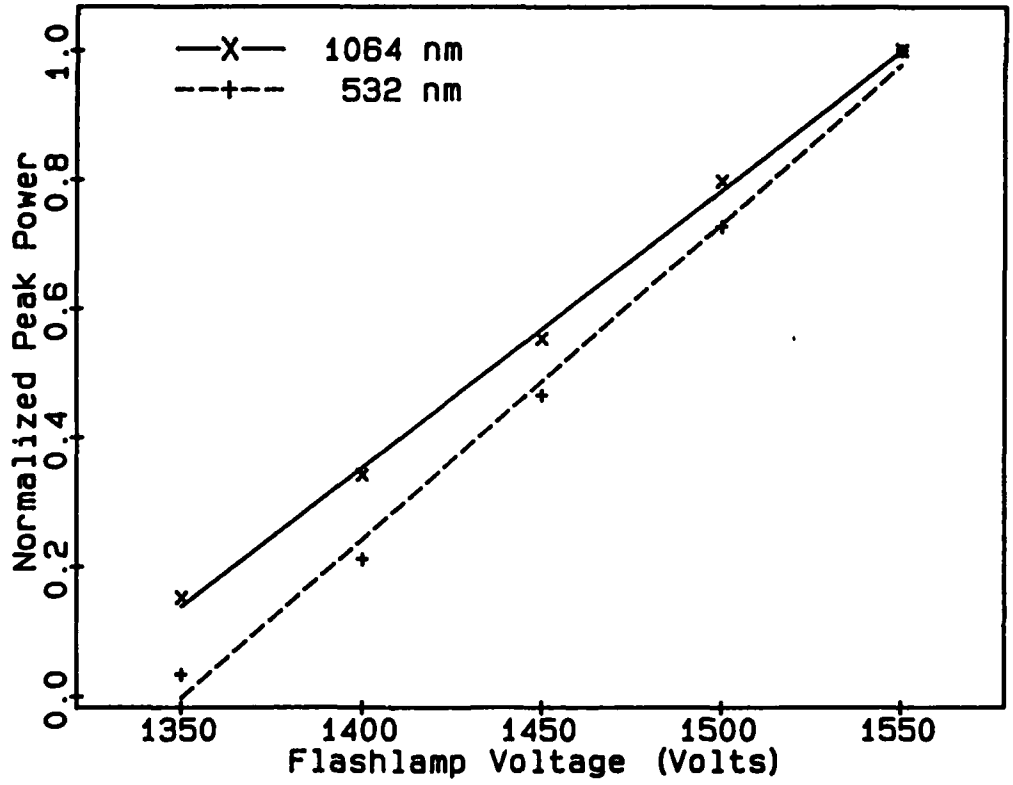

Figure 4. IR and green peak power as a function of flashlamp voltage.

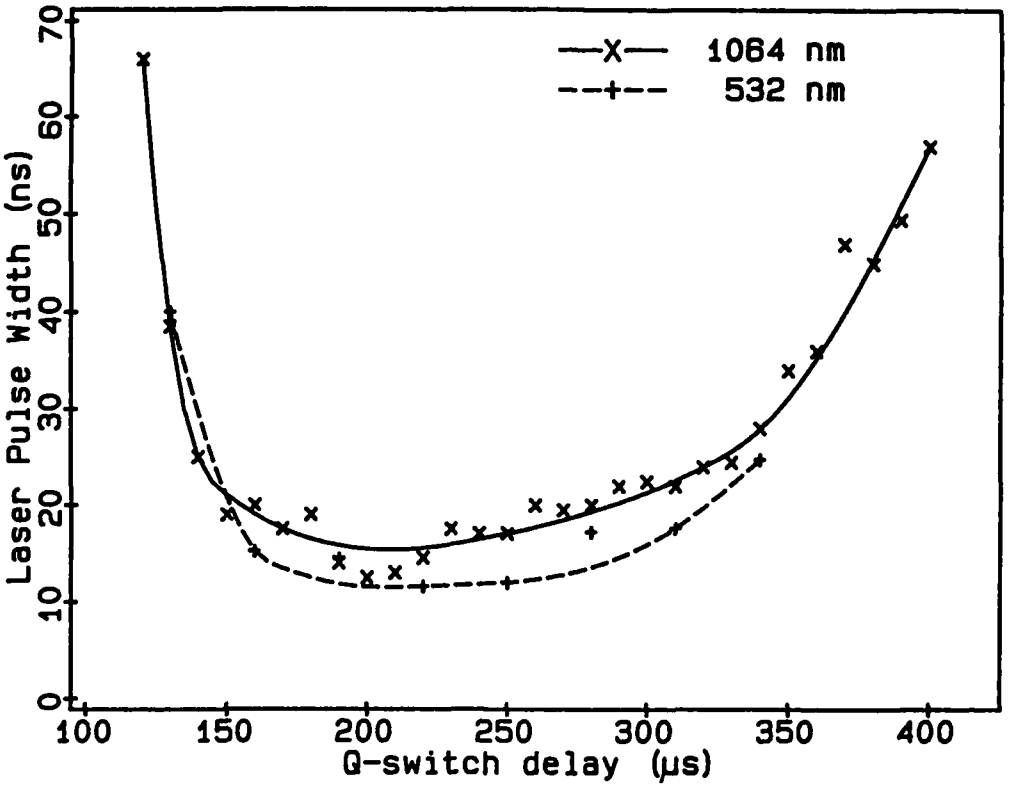

Figure 5. Temporal FWHM of the IR and green laser pulses as a function of Q-switch delay.

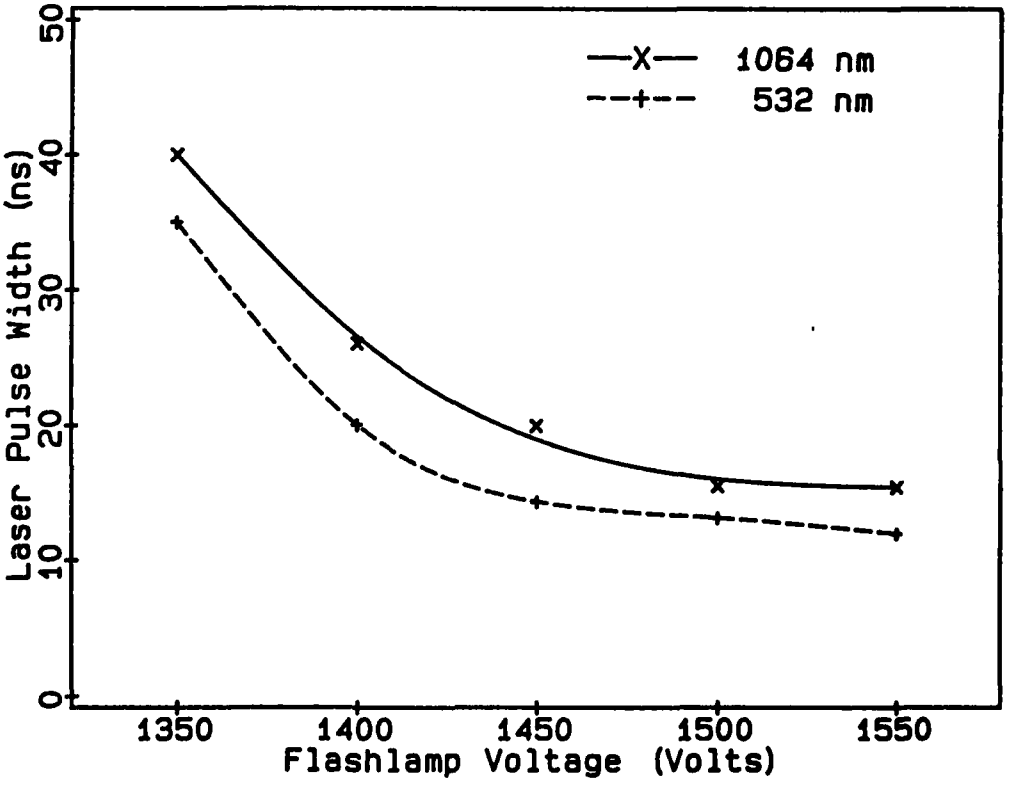

Figure 6. Temporal FWHM of the IR and green laser pulses as a function of flashlamp voltage.

silicon and to vaporize a thin ($\sim$60 nm) aluminum film off a Kapton foil. These tests indicated that at operating conditions in which the laser output was very low (either low lamp voltage, or very short or long Q-switch delays), the beam profile had a multiple-lobed pattern. Therefore, it is not practical to operate this Nd:YAG system at parameters very different from the optimum ones. The overall beam diameter was 7 mm, and during subsequent investigations a 3 mm aperture was used to define the beam and eliminate irregularities at the edge of the beam.

2. Cratering Studies

To investigate the cratering process in silicon and steel, the apparatus in Figure 7 was assembled. The fundamental 1064 nm (IR) laser beam is frequency doubled to produce 532 nm (green) radiation. The two wavelengths are separated by dichroics while the green beam is attenuated and focused before striking the target. The IR beam was also used, in which case the second harmonic generator was detuned and the dichroic separators were replaced by IR reflectors. The energy per pulse of the ablating laser beam was measured just before the lens for specific variable attenuator settings, and those same settings were subsequently used in this study.

After a series of craters were generated with a variety of laser beam parameters, depth and diameter of each crater were measured using a stylus-type surface profile measurement system. A typical crater profile (to scale), together with the definition of the parameters used in describing the craters, is shown in Figure 8.

The most significant parameter affecting the ablated craters is the power density delivered to the sample. The optical configuration, consisting of a 3 mm aperture in the $\sim$7 mm laser beam, positioned to select the most uniform part of the beam, and a 40 mm lens focused onto the sample surface, was kept the same throughout the cratering studies. Using the published beam divergence of the laser and considering diffraction through the 3 mm aperture, we estimate a focused laser spot of $\sim$ 30 μm on the sample surface. The power densities quoted below were calculated using this spot size and the measured pulse duration and energy.

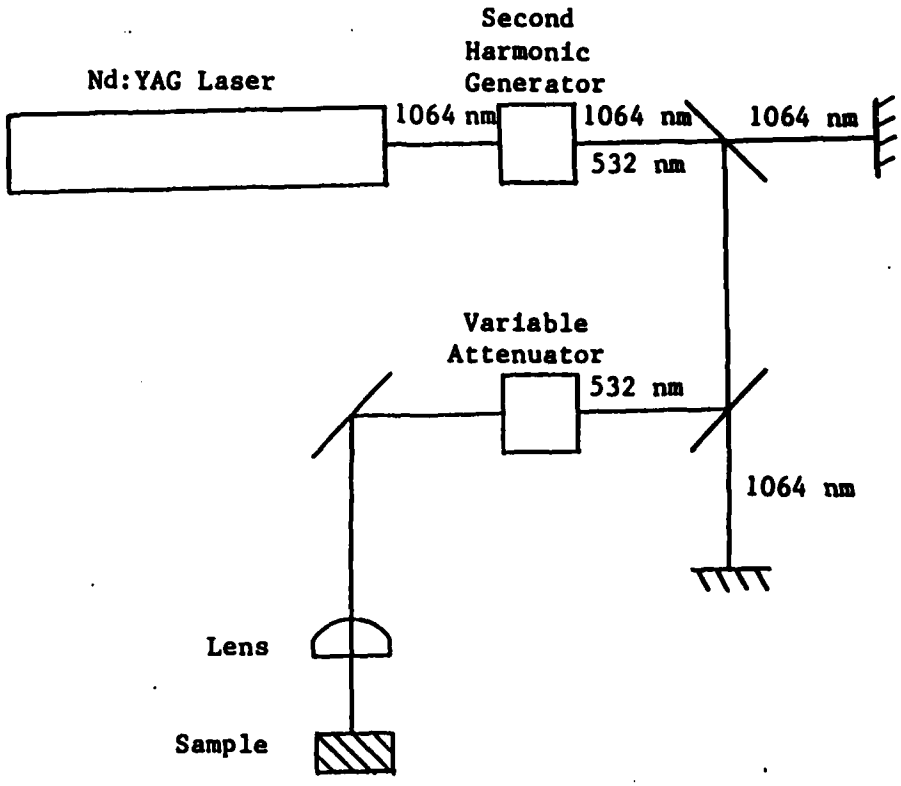

Figure 7. Schematic of apparatus assembled for cratering studies.

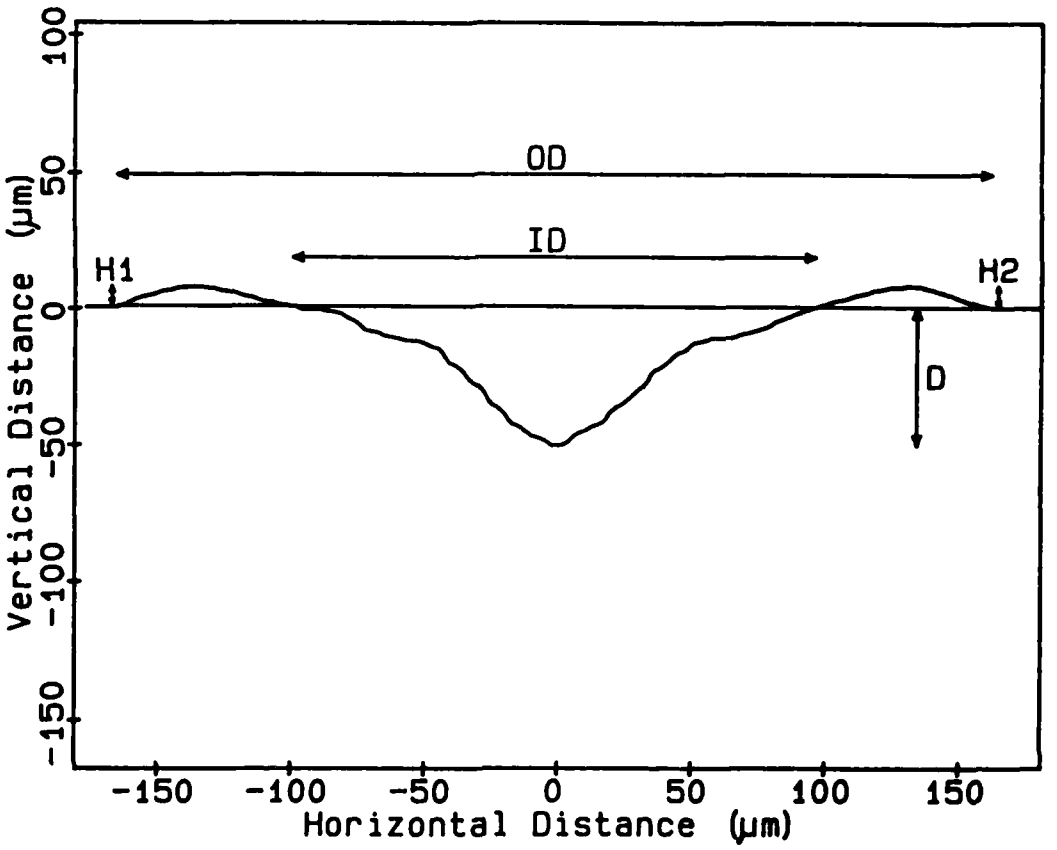

Figure 8. Scale tracing of crater profile produced in silicon after ten laser shots at 2×10^{11} W cm^{-2} indicating the parameters used to characterize the crater.

In Figures 9 and 10 are shown typical profiles of craters ablated in silicon and steel samples. (Also see Table I below.) For clarity in presentation, the depth scale is expanded by a factor of ten in these figures. As it was necessary to generate a measureable crater to reach any conclusions in this part of the study, the results discussed here are probably not directly applicable to the element analysis work described later, due to the higher power densities used. The craters in silicon, (Figure 9) were generated with a power density of 2×10^{11} W cm^{-2}, with the one shown on the left resulting after only one laser shot while ten laser shots were used to generate the crater shown on the right. Note the remarkable similarity in crater shape, with only the depth increasing with the number of laser shots.

TABLE I

Crater Parameters

(40 mm focal length lens, focused laser beam diameter ~ 30 μm)

Sample Material	Power Density (W cm^{-2})	Number of shots	OD (μm)	ID (μm)	H1 (μm)	H2 (μm)	D (μm)
Silicon	2×10^{11}	1	310	155	1.1	1.7	4.0
Silicon	2×10^{11}	10	300	165	8.5	8.0	48
Steel	7×10^{9}	10	130	50	3.9	4.4	6.9
Steel	2×10^{11}	10	230	130	7.0	8.8	24

The profile shown in Figure 10 (left) was ablated in steel with ten laser shots of 7×10^{9} W cm^{-2} each, while the one shown on the right resulted from 10 laser shots of 2×10^{11} W cm^{-2} each. In this case, there is a dramatic decrease in both crater width and depth at lower power densities. Comparing Figures 9 and 10, note that the only qualitative change in ablated crater shape occured when the power density was changed. Also note that at high power density, all the craters exhibit a crater-within-a-crater structure and that the diameter is much larger than the laser beam. Many of the observed features can probably be attributed to complex shock-wave and hydrodynamic effects in the ablation process. In fact, scanning electron micrographs of these same craters, shown in Figures 11 and 12, show remarkable similarities to impact craters

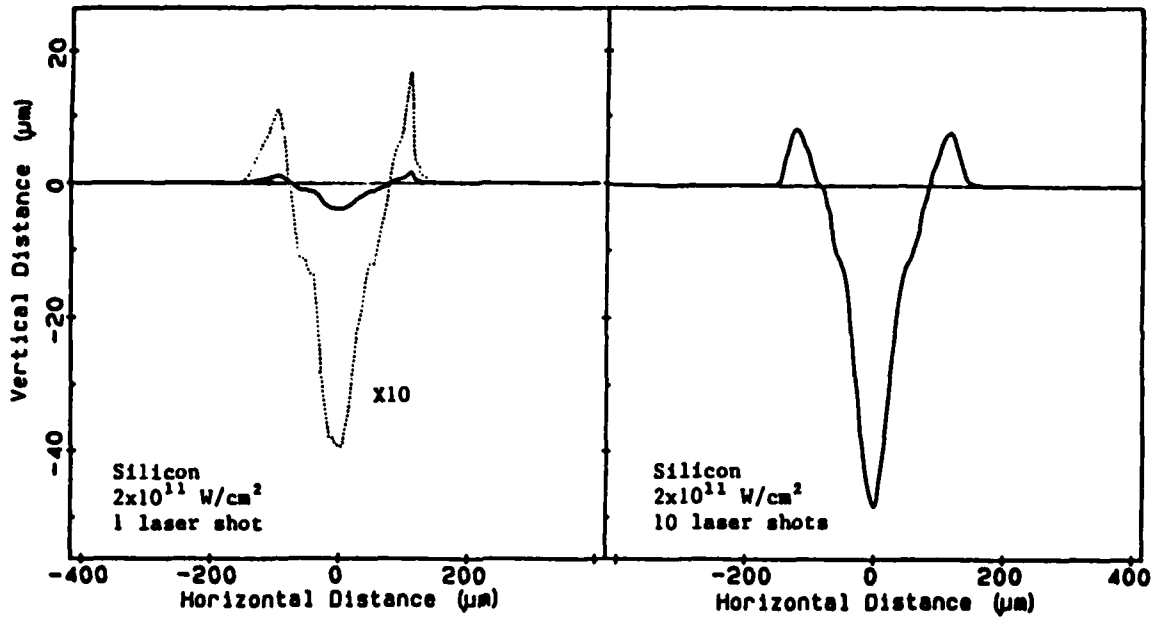

Figure 9. Typical crater profiles (vertical scale is expanded for clarity) in silicon for the same power density. Note that the crater diameter is much larger than the 30 μm laser beam and that the diameter and shape of the crater is the same after ten laser shots as it was after a single shot.

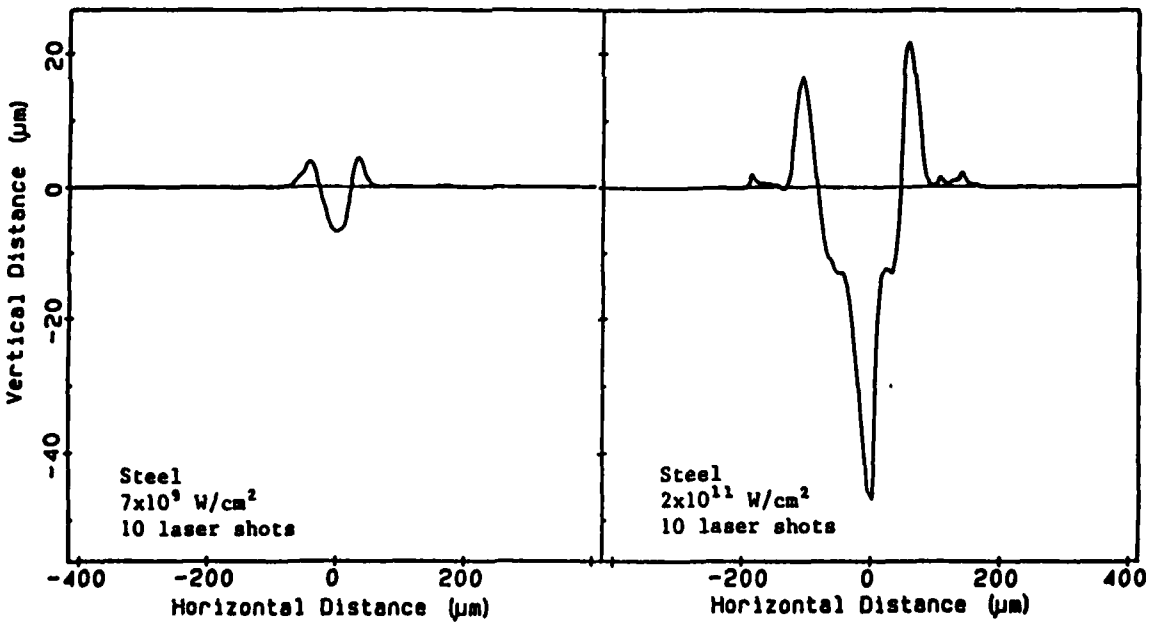

Figure 10. Craters in steel after ten laser shots at two different power densities. Note the much smaller crater diameter at lower power densities.

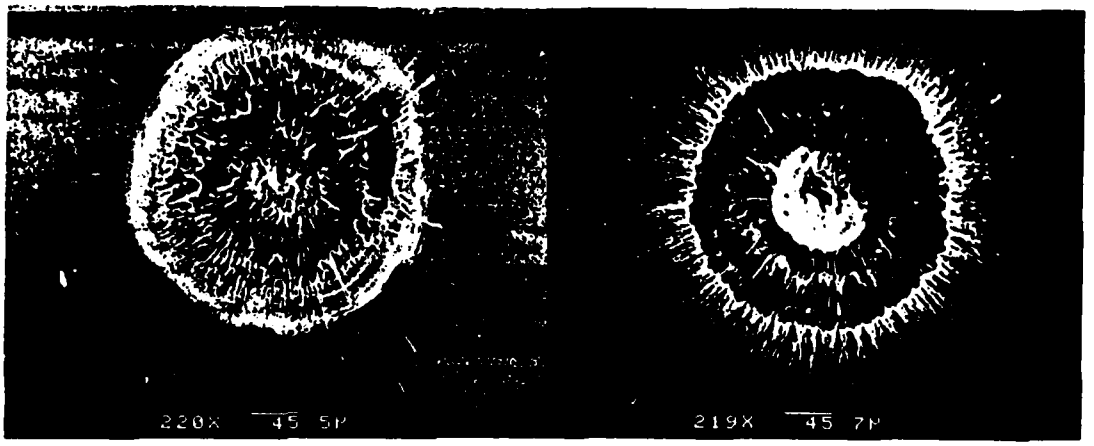

Figure 11. Scanning electron micrographs of craters produced in silicon after a single laser shot at 2×10^{11} W cm^{-2} (left) and after ten laser shots at the same power density (right). Profiles of these same craters were shown in Figure 9.

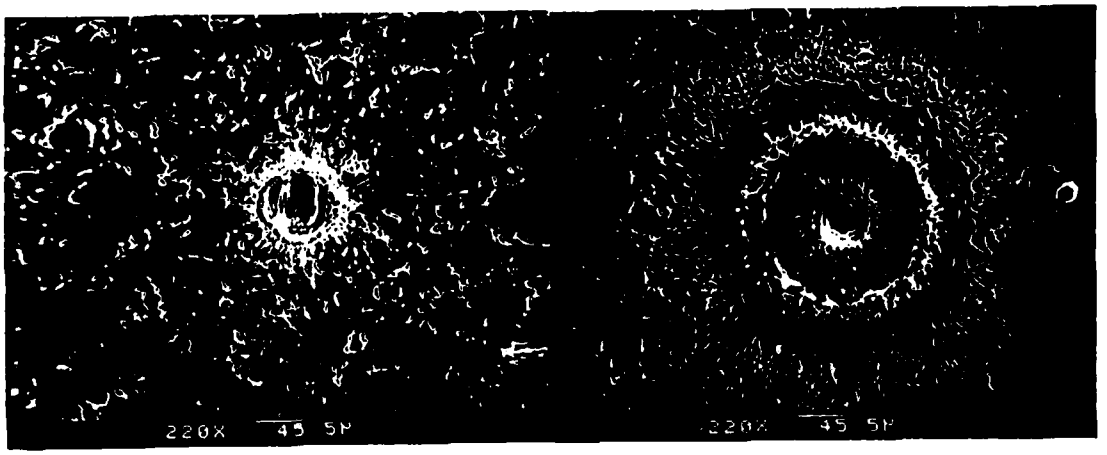

Figure 12. Scanning electron micrographs of craters produced in steel after ten shots at 7×10^{9} W cm^{-2} (left) and after ten shots at 2×10^{11} W cm^{-2} (right). Profiles of these same craters were shown in Figure 10.

seen on lunar and planetary surfaces. At the lower power densities used in the analysis of the samples, (discussed in Section IV.4) marks, if any, left on the samples were approximately of the same size as the ablating laser beam.

Profiles were obtained for craters produced using a variety of laser beam parameters: 15 and 45 ns pulse widths, 40 and 300 mm focal length lenses (each located for best focus of the beam onto the sample), 1 to 300 shots, 2×10^8 to 2×10^{11} W cm^{-2}, and 1064 nm and 532 nm wavelengths. The pulse width was increased from 15 ns (minimum) to 45 ns by changing the Q-switch delay time. This decreased the energy per pulse and power density, which predictably resulted in craters of smaller depth and diameter. No effects due to the pulse width itself could be measured. Similarly, using the longer focal length lens increased the beam diameter at the sample and hence reduced the power density, but no significant effects attributable to parameters other than power density could be discerned.

The dependence of the crater depth on the number of laser shots is shown in Figure 13 for craters in silicon (upper) and steel (lower) using the 1064 nm fundamental laser wavelength and two different power densities for each material. The depth increases linearly with the number of shots in each case, although there is some scatter in the data, probably due to shot-to-shot variations in laser intensity. The 532 nm laser wavelength (Figure 14) was also used at two different power densities, one greater and one less than the power densities used at 1064 nm. Again, the depth dependence is linear with the number of shots in each case. Although the effects of the two different wavelengths have not been compared directly, no obvious wavelength dependence can be found for this data.

It should be noted that the power densities used here are much larger than those used for sampling in the time-of-flight mass spectrometer (Section IV.4). It was determined experimentally that an ablation power density of only 4×10^7 W cm^{-2} was sufficient to obtain a strong signal for impurity concentrations below 1 ppm. This is well below the damage threshold for either silicon or steel, and no crater diagnostics were possible at these power densities.

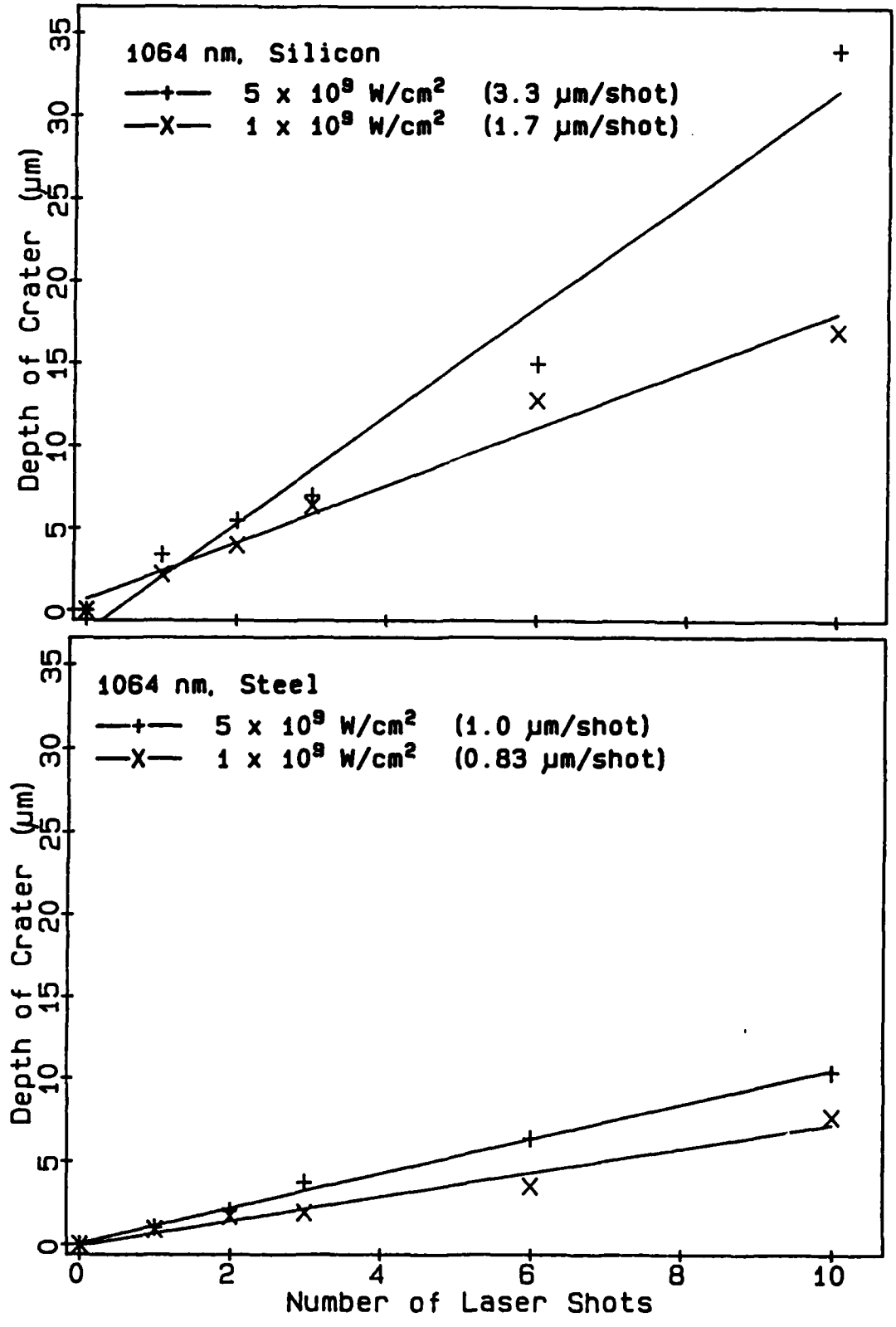

Figure 13. Dependence of crater depth on number of laser shots at 1064 nm in silicon (upper) and steel (lower) for two values of incident power density.

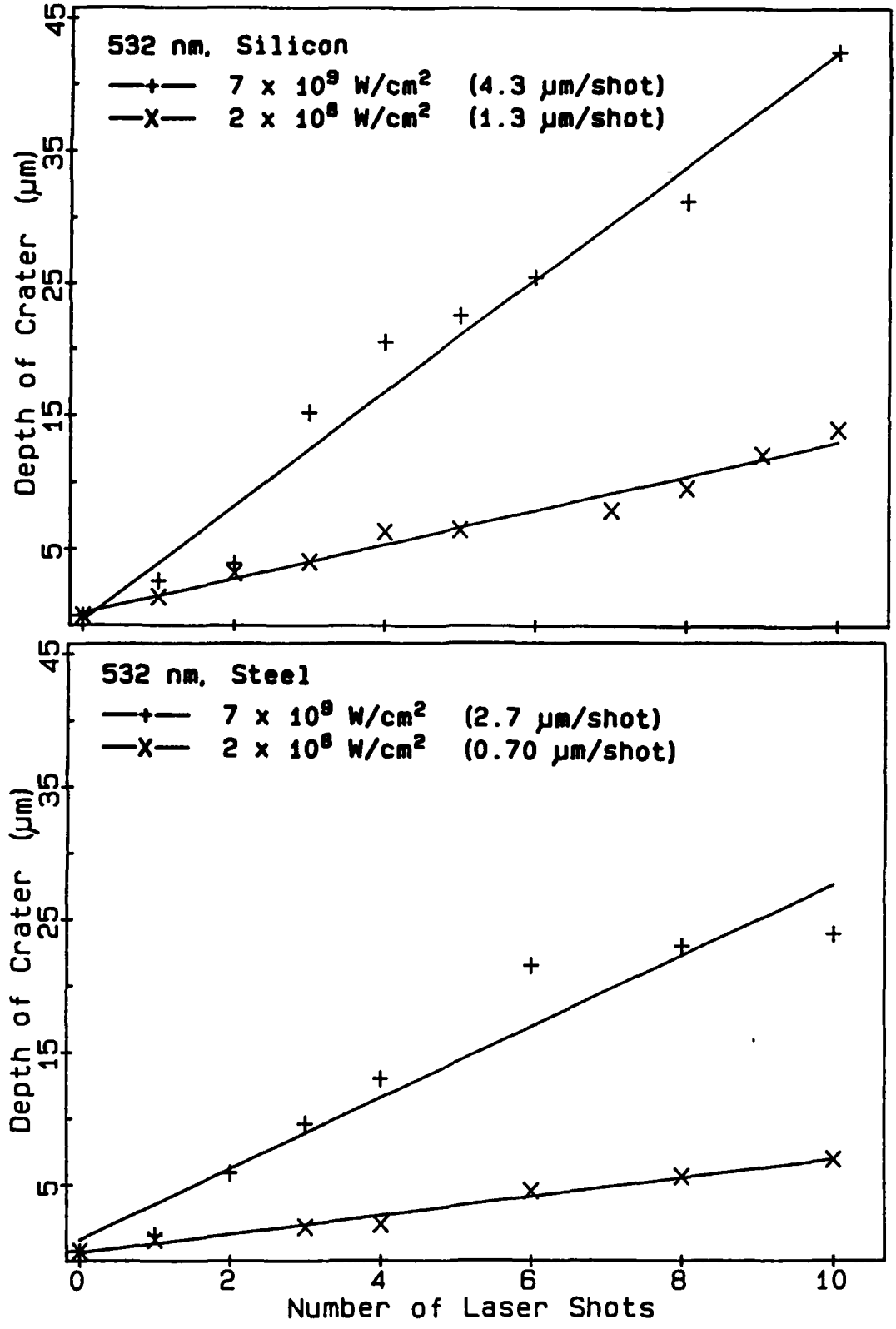

Figure 14. Dependence of crater depth on number of laser shots at 532 nm in silicon (upper) and steel (lower) for two values of incident power density.

3. System Description

The experimental apparatus consisting of a Nd:YAG ablation laser, a RIS laser system, and a time-of-flight mass spectrometer is shown schematically in Figure 15. In all of these measurements, ablation laser flashlamp voltage of 1500 V, Q-switch delay of 190 us, and 532 nm wavelength was used. After passing through a 3 mm aperture, the laser beam was focused onto the sample with a 300 mm lens, yielding a 150 μm spot. Ablation power densities were between 8×10^6 and 3.5×10^7 W cm^{-2} for data acquisition and between 2.5×10^8 and 6×10^8 W cm^{-2} for in-situ sample cleaning prior to analysis (see Section IV.4). The appropriate power density for data acquisition was determined experimentally in each case by adjusting the variable attenuator while monitoring the TOF signal. The actual power density used was calculated from the pulse energy (calibration curve of Figure 16), the measured pulse duration, and the area of the focused ablation laser spot.

For this feasibility study, measurements were limited to only two analytes: gallium and aluminum, both of which can be ionized using similar RIS schemes, as shown in Figure 17. In each case, the excitation step is accomplished using a resonant ultraviolet (UV) photon, while the ionization step uses the infrared (IR) fundamental wavelength of the Nd:YAG pump laser. The two beams are combined using a dichroic reflector before passing colinearly and simultaneously through the ionization region.

The TOF mass spectrometer (Figure 18) was designed in the standard two-stage Wiley-McLaren configuration (13), modified to accommodate a solid sample and the ablation laser beam. The sample stage was mounted on an off-axis rotary feedthrough, allowing different positions on the sample to be moved into the focal spot of the ablation laser beam. A dual microchannel plate detector with 50 ohm anode was used to provide a flat detector plane and preserve the time resolution of the TOFMS. The detected signal was amplified using a fast preamp and amplifier and digitized with a transient recorder having 10 ns resolution. The transient recorder and a programmable delay generator are part of a microprocessor-controlled CAMAC

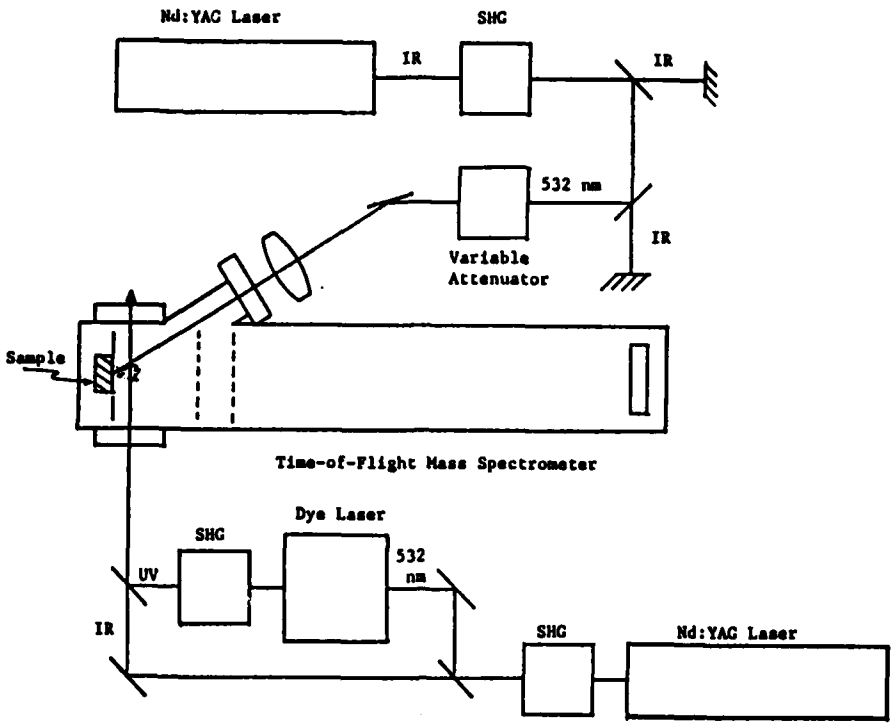

Figure 15. Schematic of the system used in this study. The ablation laser beam strikes the sample with near-normal incidence, while the RIS laser beams ionize the expanding plume after a short delay.

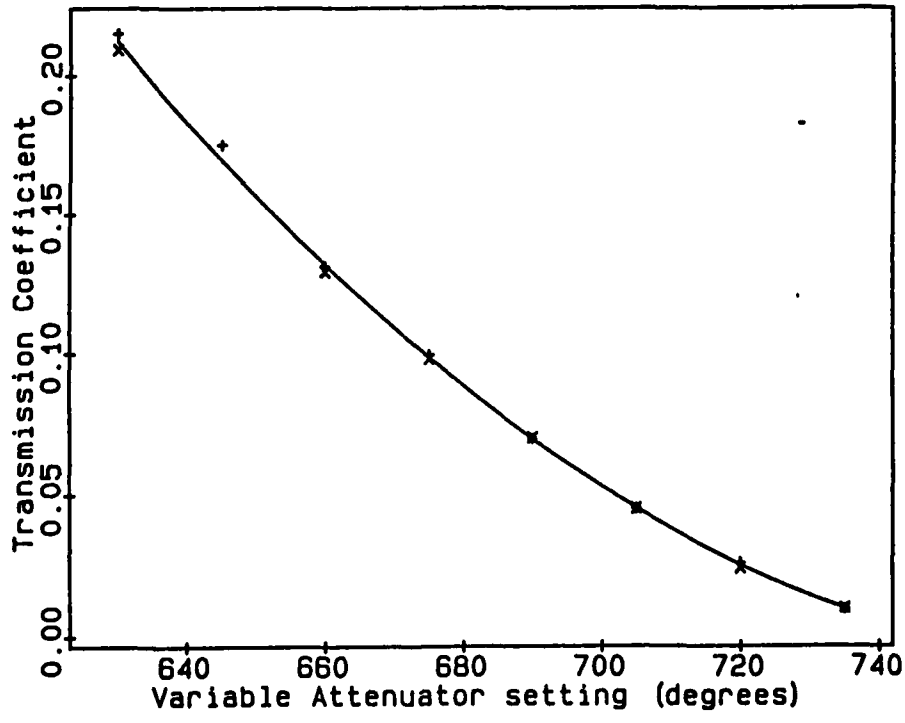

Figure 16. Calibration curve for the variable attenuator.

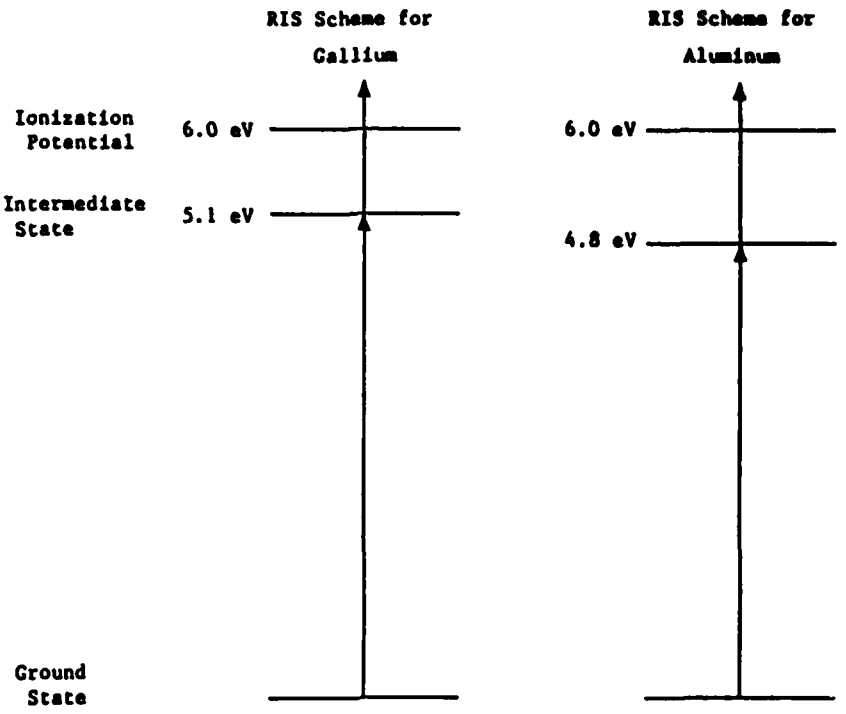

Figure 17. RIS schemes used in this study for gallium and aluminum.

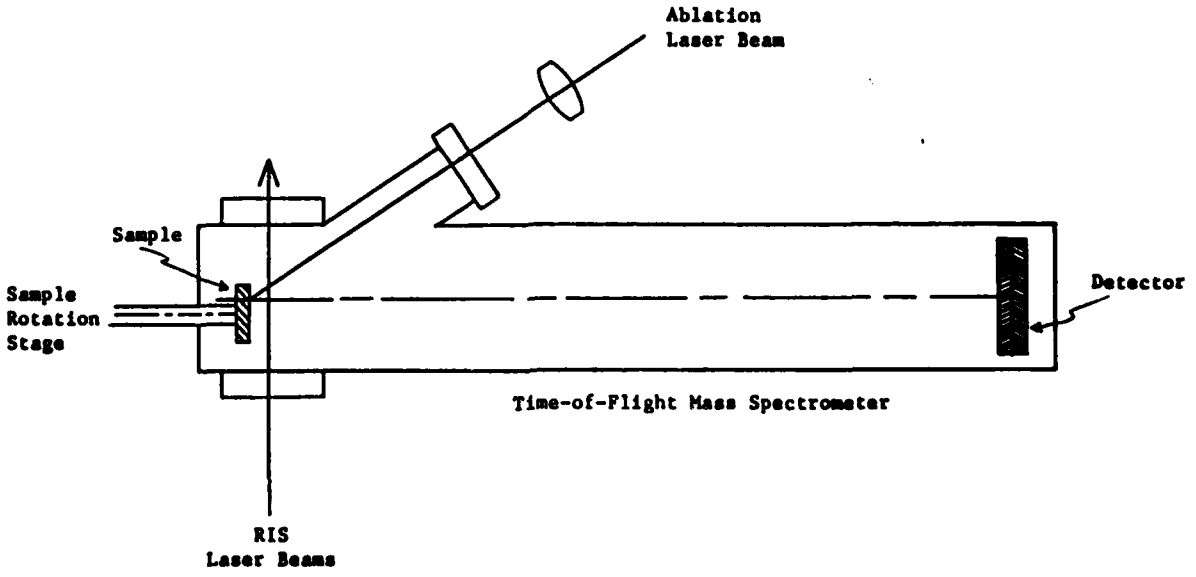

Figure 18. Detail of the sample interaction region, showing the rotation stage, allowing up to four samples to be mounted and analyzed at many locations without opening the system.

data acquisition system which is also interfaced to a main computer for data storage and analysis.

The data acquistion software, previously developed at Atom Sciences, provides powerful and convenient control over data acquisition and analysis parameters. A particularly useful software feature is the thresholding capability, rejecting all data below an adjustable preset value. This enables effective discrimination against electronic noise by only accepting ion arrivals. Wide dynamic range is achieved by storing both the amplitude of the detected ions and the number of individual detections, thereby utilizing analog data accumulation for high-level signals while simultaneously utilizing single-ion counting for weak signals.

Figure 19 shows the timing sequence during normal data acquisition. The flashlamps for both the ablation and RIS Nd:YAG lasers fire simultaneously. The digital delay, here set to 190 μs, triggers the ablation laser Q-switch at the optimum time, initiating the ablation process and creating neutrals and ions which are accelerated. This signal we shall refer to as the ablation TOF mass spectrum. After a second adjustable delay, between 1 and 10 us, the Q-switch for the RIS Nd:YAG laser is triggered. (As was shown in Figure 5, from Section IV.1, the laser output changes only slightly for delay times within 30 μs of the optimum.) This delay is adjusted to maximize the number of ablated atoms in the ionization region when the RIS lasers are fired. The RIS ions are also accelerated, generating a RIS TOF mass spectrum which overlaps the ablation TOF mass spectrum, offset by the above delay time. Therefore the RIS TOF signal of interest could potentially suffer from interferences due to heavier mass peaks in the ablation TOF mass spectrum; an example of this is given in the following section, along with two suggested techniques for eliminating the interference. The transient recorder is triggered after a third independently adjustable delay, and can acquire and transfer to the microprocessor up to 2048 data points at 10 ns intervals for each laser pulse at 10 Hz. This 20 μs range corresponds to mass numbers 0 to 130 in the RIS TOF mass spectrum using the present voltages. Most often, only the mass range including the analyte is of interest, and fewer data points are required.

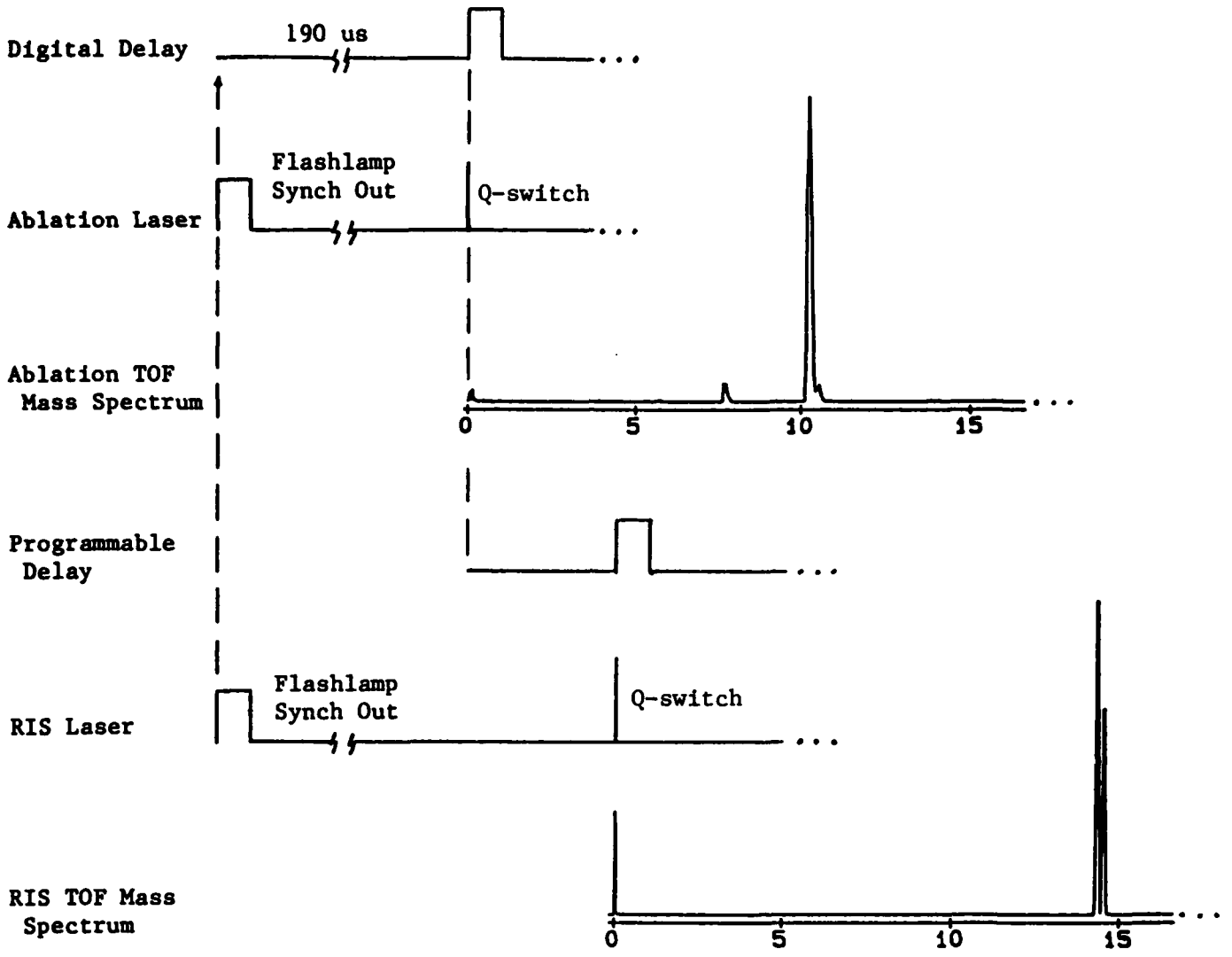

Figure 19. Timing sequence showing the triggering of the ablation laser and the RIS laser at the appropriate times. Note that the ablation TOF mass spectrum and the RIS TOF mass spectrum have different starting times; the two spectra are shown separately for clarity, but in fact the detector records a superposition of both.

4. Time-of-Flight Data

Preliminary data acquisition provided the necessary diagnostic information required to optimize the parameters and techniques for proper sample analysis. Figure 20 shows the mass spectrum of a silicon sample analyzed for gallium, which was present at the 58 ppm level. The RIS scheme for gallium uses a UV photon for the single excitation, followed by ionization with the IR fundamental beam from the Nd:YAG laser. The first peak results from UV photons scattered onto the detector, providing a convenient marker for t=0. The next three peaks are from ions formed in the ablation process, occuring 5.5 μs before the RIS lasers fire. The peaks are identified as ^{23}Na (100% isotopic abundance), and ^{39}K and ^{41}K (93% and 7%, respectively). The peaks just before 15 μs should be the RIS signals from ^{69}Ga and ^{71}Ga, but the isotope abundances should be 60% and 40%, respectively, whereas the data show the first of the two peaks smaller than the second. The discrepancy is resolved by changing the delay time between the ablation laser and the RIS laser from 5.5 μs to 5.0 μs, as shown in Figure 21. The TOF for the gallium peaks is still just less than 15 μs, but the entire RIS TOF mass spectrum is shifted with respect to the laser ablation TOF mass spectrum, thus separating the previously overlapped peaks. The laser ablation peak, which occurs at about 15 μs on the RIS TOF scale and about 20 μs on its own laser ablation TOF scale, is now identified as ^{133}Cs (100%). The decrease in RIS signal between Figure 20 and Figure 21 results mostly from surface effects which cause strong fluctuations in the ablation rate. Cleaning of the surface, as discussed below, can significantly reduce this problem.

In the above example, the peaks in the ablation TOF mass spectrum were from easily ionized alkali metals, which are commonly present on surfaces exposed to outside or normal laboratory environments. Sample surfaces also commonly develop a layer of oxide or adsorbed oxygen and water vapor, which tend to reduce the density of ablated neutral atoms available for resonance ionization. In-situ cleaning of the sample is an effective technique for obtaining a fresh surface for analysis, and can be

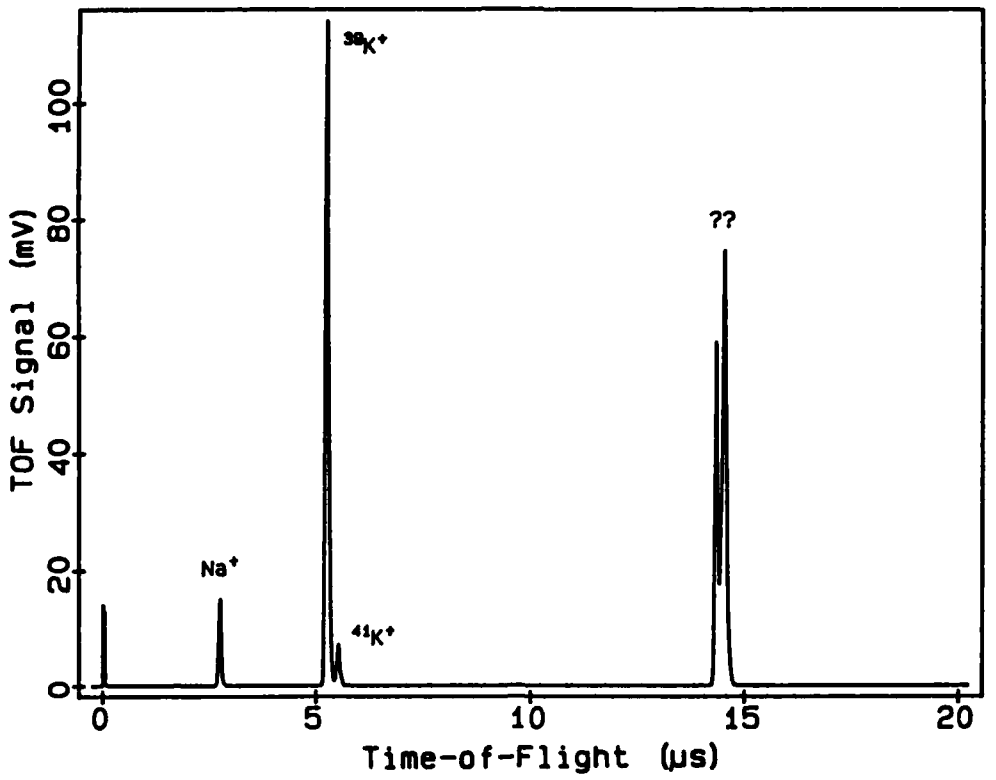

Figure 20. TOF mass spectrum showing superposition of ions created in the ablation process and by RIS.

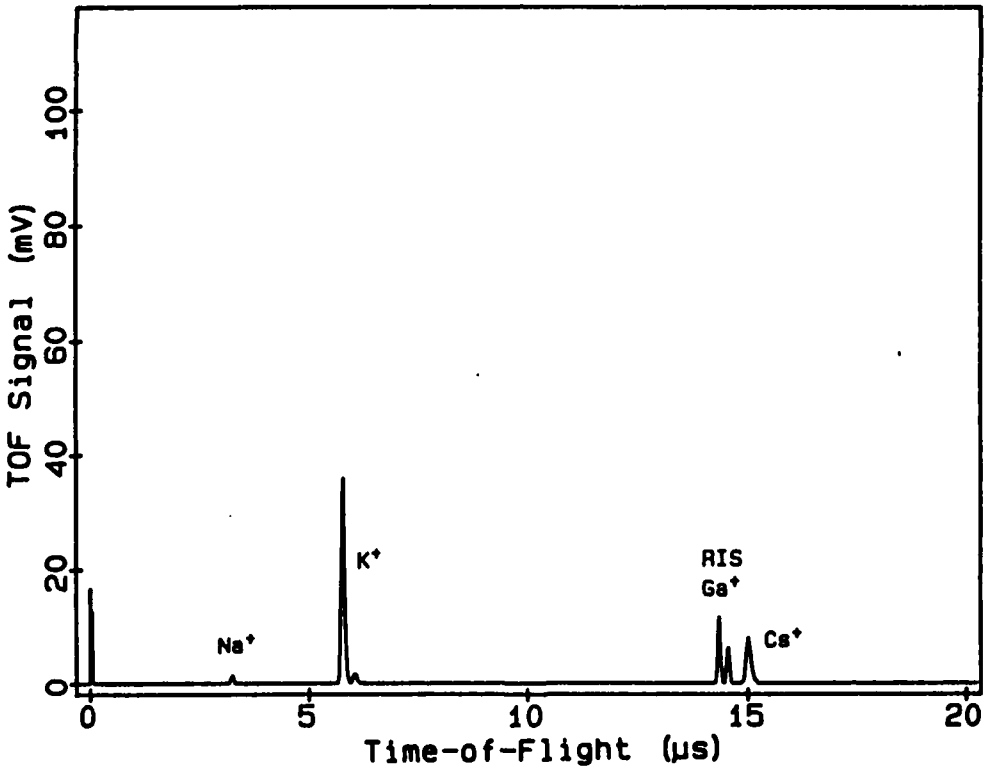

Figure 21. Separation of the ablation ions from the RIS ions by changing the delay between the two lasers. The Ga^+ isotope ratios now appear to be correct.

accomplished by electron or ion sputtering, although in this experiment it is more convenient to use higher laser intensity to remove the surface layer. Figure 22 shows the mass spectrum for the 58 ppm Ga in Si sample, both before cleaning (top trace) and after cleaning for 5 seconds (bottom trace). For this data, the laser intensity was 2.5×10^7 W cm^{-2} during analysis and 2.5×10^8 W cm^{-2} during cleaning. This simple cleaning technique essentially eliminates the alkali laser ablation signals and enhances the RIS signal of Ga by a factor of 50. Similar data is shown in Figure 23 for a National Bureau of Standards (NBS) Standard Reference Material (SRM) of stainless steel containing 2400 ppm Al, by weight. In the top trace (before cleaning), the first two peaks are laser ablation signals for ^{39}K and ^{41}K, and the third small peak is the RIS signal for ^{27}Al, which occurs later because the RIS laser pulse occurs 3.5 μs after the ablation laser pulse. After cleaning for 10 seconds at 2×10^8 W cm^{-2} (bottom trace), the potassium signals have again been eliminated. The ablation laser intensity used for analysis was 8×10^6 W cm^{-2} for the top trace and 2×10^7 W cm^{-2} for the bottom trace.

To demonstrate the selectivity of the RIS technique, a silicon sample with 58 ppm gallium was analyzed with the excitation laser wavelength both off-resonance and on-resonance. The on-resonance Ga signal is shown in the bottom trace of Figure 24, while the top trace shows the signal with the excitation laser off-resonance by 0.073 nm. Note that the vertical scale is expanded by a factor of 200. The total gallium signal has been reduced by a factor of at least 5000, and should be smaller for wavelengths further from resonance. Thus the selectivity of RIS is high, and can be optimized for particular analyses by proper choice of wavelengths. Note in particular that the nonresonant ionization signal from the silicon matrix material is at most 0.013 mV, which when compared with the 153 mV ^{69}Ga signal and the 2.9×10^4 ^{28}Si:^{39}Ga abundance ratio, yields a laser ionization efficiency (assuming that the entire signal in the mass 28 channel is from Si) that is at least a factor of 3×10^8 greater for gallium than for silicon.

The high signal strength and simplicity of the RIS TOF mass spectrum in Figure 24 (lower) can be directly compared with the weak and complicated mass spectrum from the laser ablation ions as seen in Figure 25, where the RIS lasers have been blocked. In the RIS TOF mass spectrum of Figure 24,

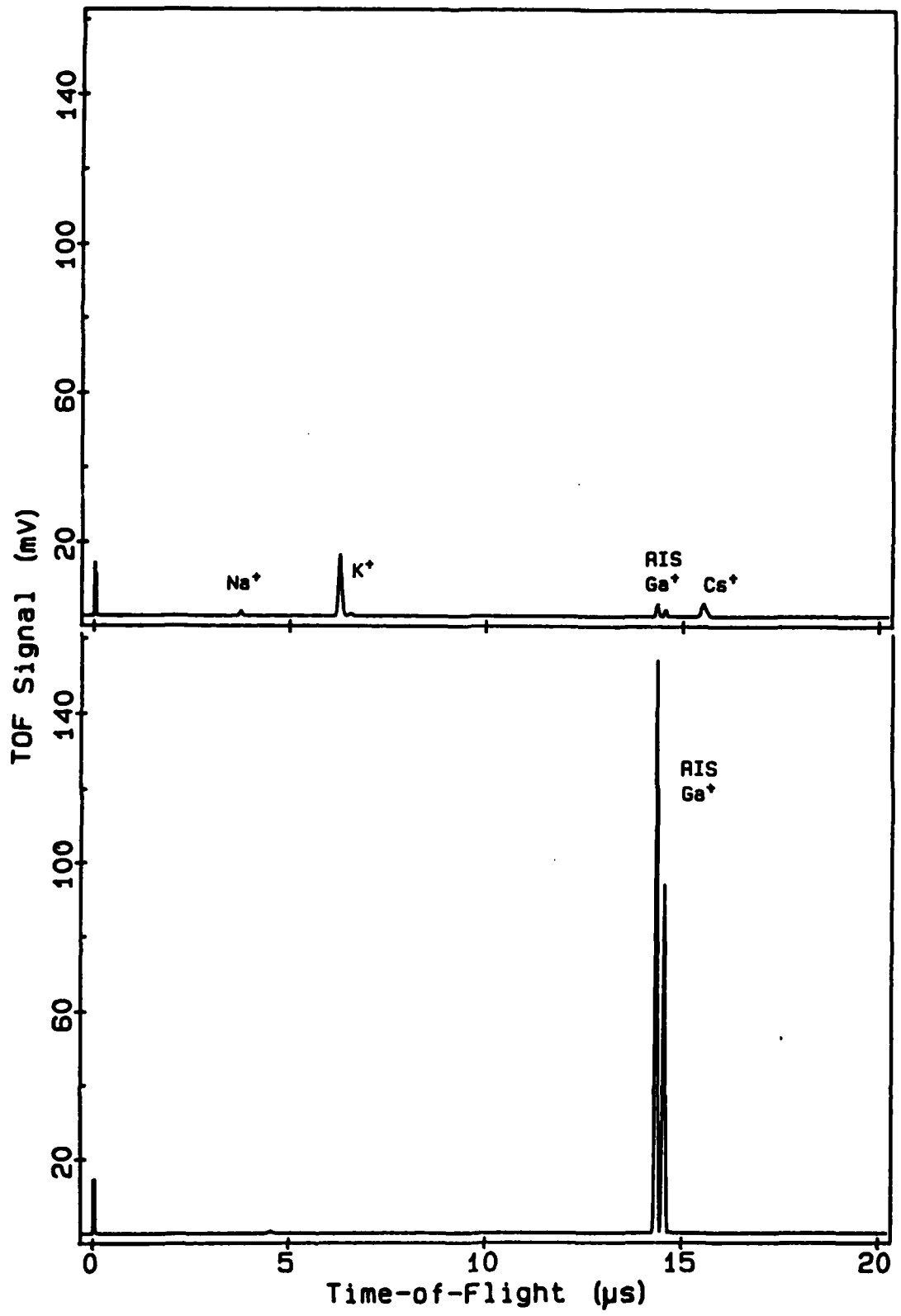

Figure 22. TOF mass spectrum from a 58 ppm Ga in Si sample before cleaning the sample surface (upper) and after cleaning for 50 laser shots (lower) by irradiating the sample at ten times the power density used during analysis. Note the dramatic increase in RIS signal and virtual elimination of all interferences.

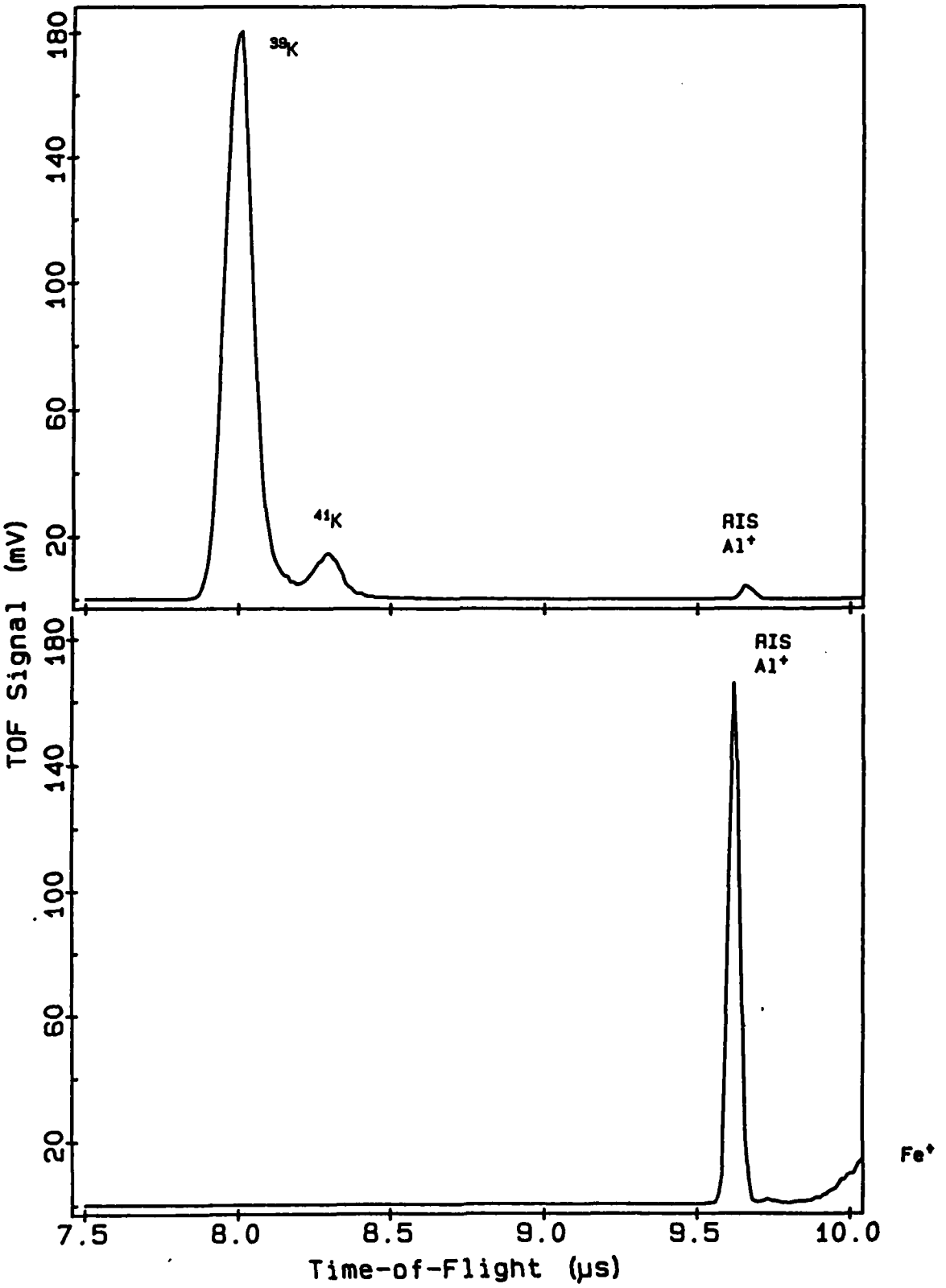

Figure 23. TOF mass spectrum of a steel sample containing 2400 ppm Al before cleaning (upper) and after cleaning (lower). Again note the significant increase in RIS signal and elimination of K^+ ablation signal.

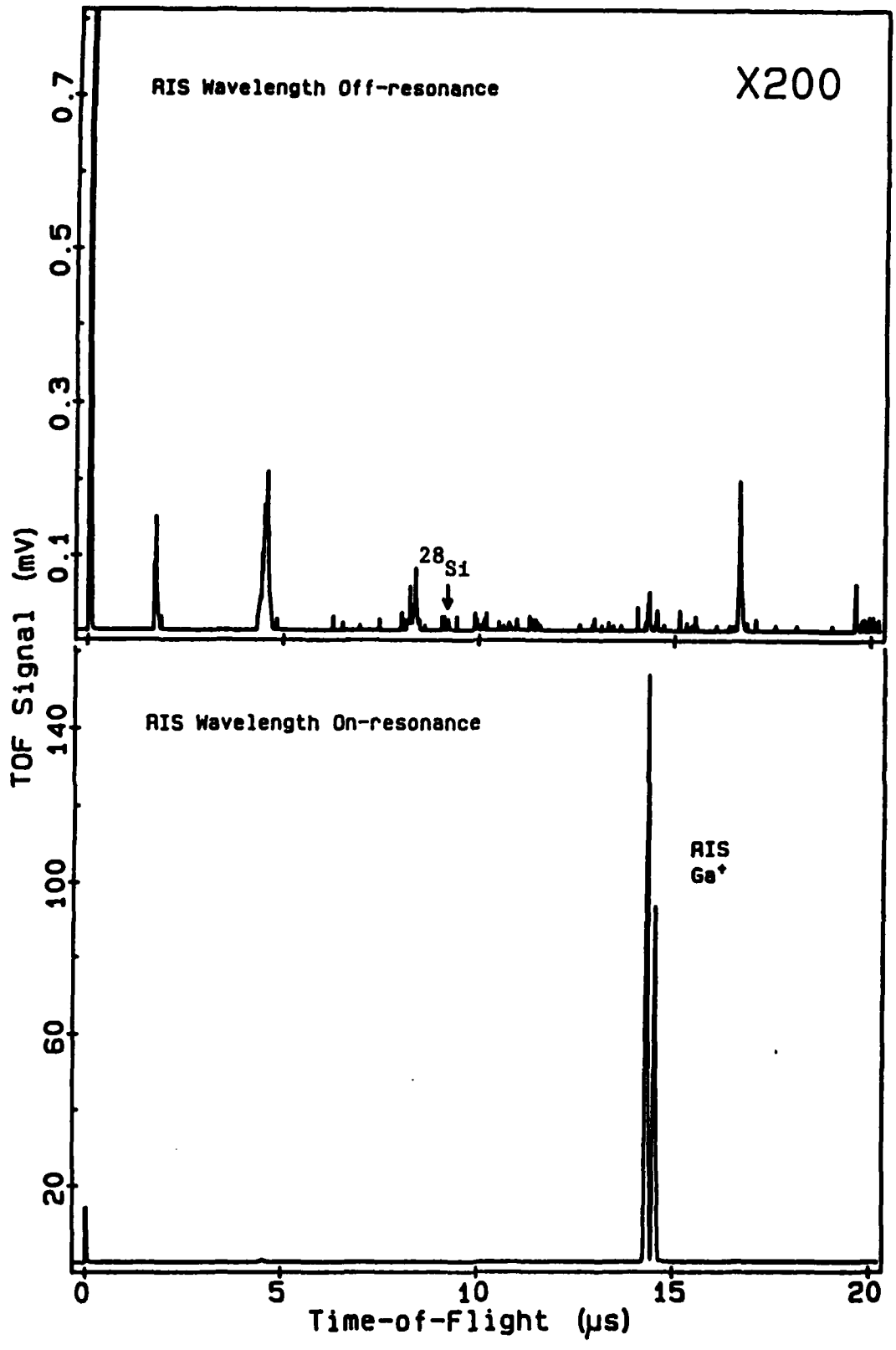

Figure 24. Selectivity of the RIS process, showing the very weak Ga^+ signal when the RIS laser was 0.07 nm off-resonance (upper) compared to the on-resonance signal (lower). Note that the sample is 100% Si, with only 58 ppm Ga.

the two ^{69}Ga and ^{71}Ga peaks (from gallium at the 58 ppm level) are clean and well resolved, while the laser ablation ions, essentially all due to the matrix silicon (Figure 25), show a weak and complicated spectrum. This comparison attests to the significant advantages of the RIS technique. The sensitivity of the RIS technique is shown in Figure 26, in which very good signal to noise ratio is achieved after only 500 laser shots for a 0.48 ppm Ga in Si sample. The amount of material removed by the ablation laser was so small that no visible mark was made on the sample.

5. Correlation Studies

For laser ablation to be useful as the sampling method for an analytical technique, the signal vs. concentration relationship for the system should be known, reproducible, and preferably linear. To measure this relationship, we analyzed silicon samples with well-known concentrations of gallium and steel samples with aluminum concentrations certified by the National Bureau of Standards (NBS). A log-log plot of signal vs. concentration gives a slope of one (45 degrees) for perfectly correlated data.

We measured the Ga RIS TOFMS signal for four silicon samples having Ga concentrations of 0.48 to 58 ppm, both before and after cleaning of the samples using increased laser power density (Section IV.4). In each case, the ablation power density used for analysis was the same for all four samples, and the amplifier gain was adjusted for each sample to give measurable signals without saturating the transient digitizer. For each individual measurement, the time-of-flight signal was summed over 500 laser shots (50 sec at 10 Hz), then integrated over the mass peaks for the two gallium isotopes. Ten measurements were made sequentially for each sample. The individual data points (+) and the averages (circles) are plotted vs. concentration in Figure 27, for the samples before cleaning (upper plot) and after cleaning (lower plot). A comparison of the two plots indicates that cleaning is effective not only for making the system response more linear, but also for decreasing the scatter in the data. For this data, the ablation laser power density was 3×10^8 W cm^{-2} for cleaning (50 laser shots) and 2×10^7 W cm^{-2} for data acquisition.

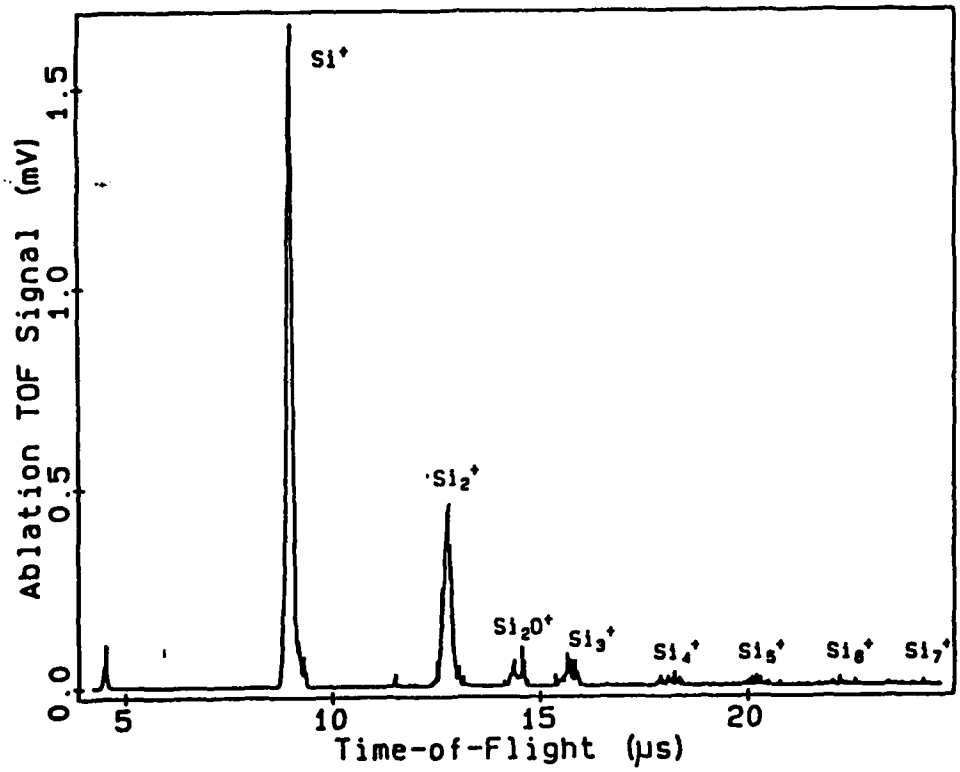

Figure 25. Ablation TOF signal from the same 58 ppm Ga in Si sample shown in Figure 24, showing the complex mass spectrum seen from the silicon matrix alone. As no RIS lasers were used in this run, the start time occurs 4.50 μsec earlier.

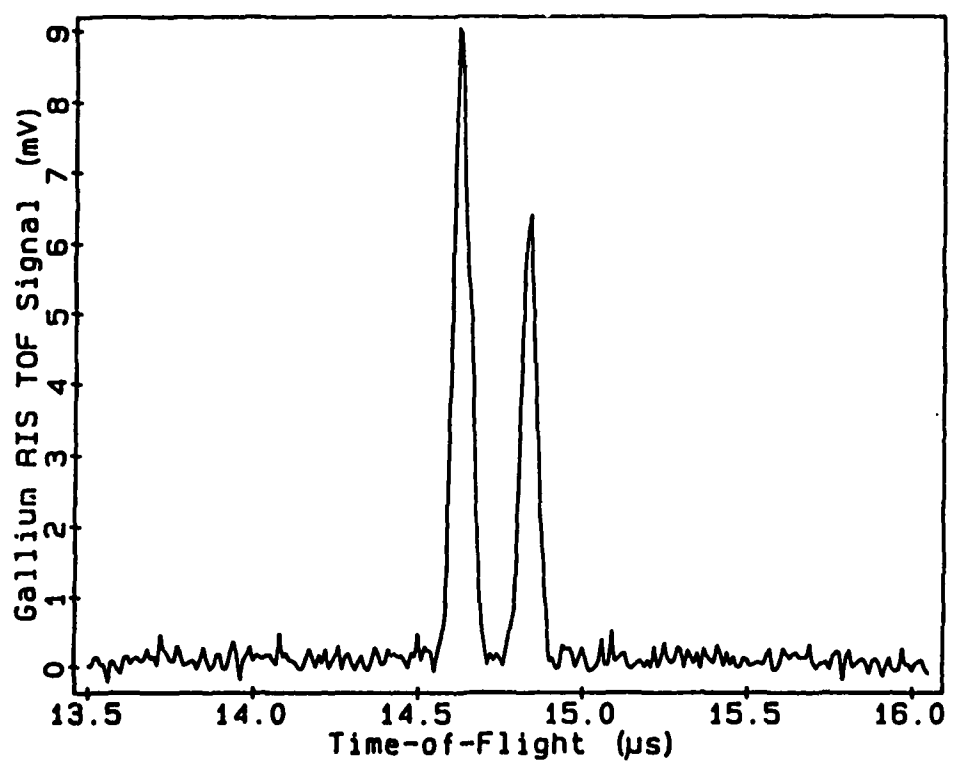

Figure 26. Gallium signal seen after only 500 laser shots from a sample containing 0.48 ppm Ga in Si. The sensitivity derived from this data is 15 ppb. Simple operational changes could increase the sensitivity to at least 0.1 ppb.

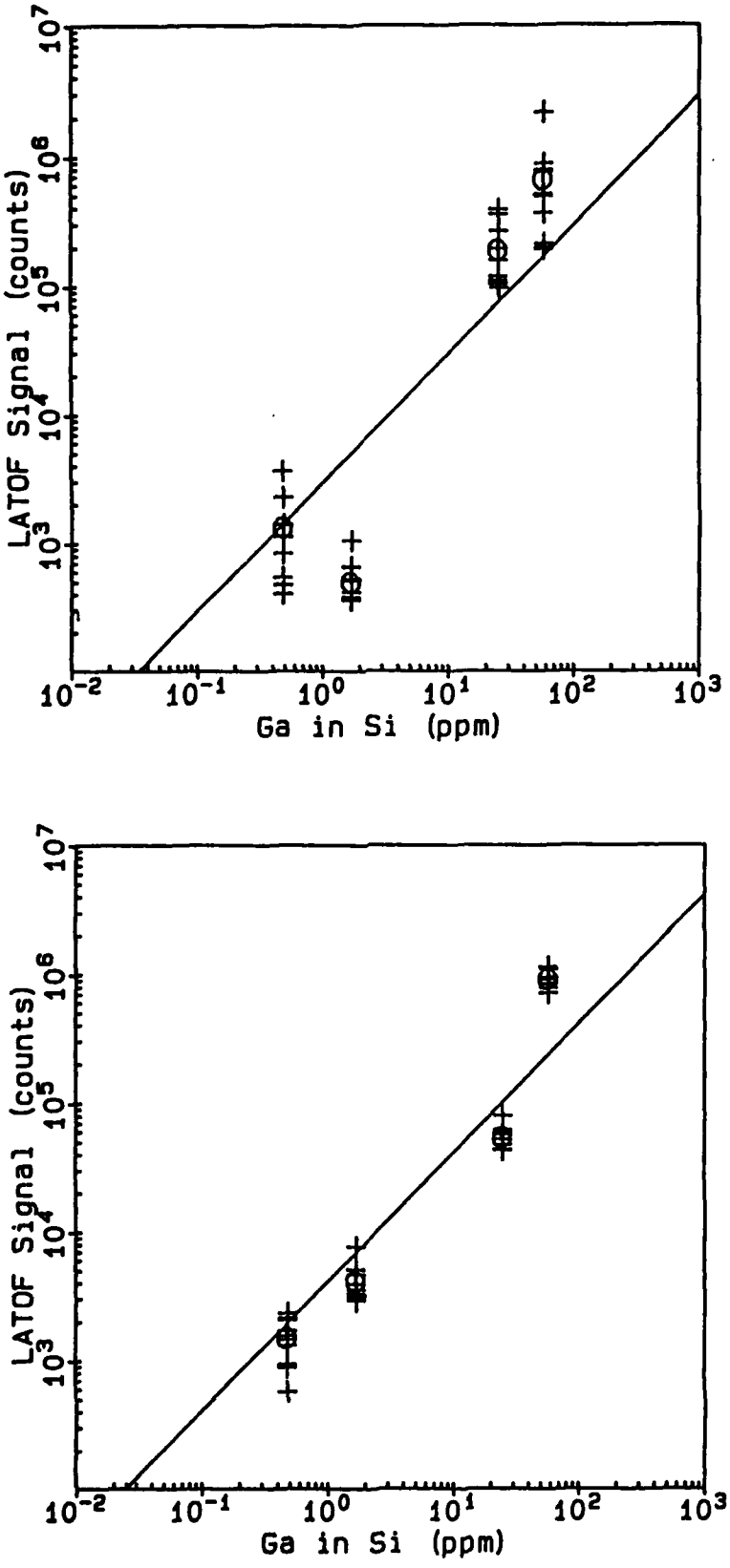

Figure 27. Correlation of the Ga RIS signal with Ga concentration before cleaning (upper) and after cleaning for 50 laser shots at ten times the analysis power density (lower). Note the reduced scatter and improved correlation with concentration. The crosses are individual 500 shot analyses, while the circles are the averages.

The NBS steel samples were analyzed for aluminum three times: first with no cleaning and 6×10^6 W cm^{-2} for analysis, next after cleaning 10 sec (100 laser shots) at 3×10^8 W cm^{-2} using 3×10^7 W cm^{-2} for analysis, and finally after another 10 sec cleaning at the same power density and with 4×10^7 W cm^{-2} for analysis. The three corresponding correlation plots are shown in Figure 28. The Al RIS signals for the steel samples showed considerable scatter in the individual measurements before cleaning and essentially no correlation to the certified concentrations. Cleaning the samples reduced the scatter for three of the four samples, and the averages moved toward the correlation line. Moving to a new spot on each sample and cleaning again yielded about the same results for the averages, with somewhat more scatter than before.

Although the correlation was not good for these samples, the consistent averages after cleaning suggest a systematic effect. Note in particular that the 7 ppm Al sample, even though having the smallest signal variation, is farthest from the correlation line. Possible errors may be due to cross-contamination from higher concentration samples, or perhaps to surface segregation of the aluminum before or during cleaning. The peculiar surface condition of the 7 ppm Al sample after analysis is shown in the scanning electron micrographs of Figure 29.

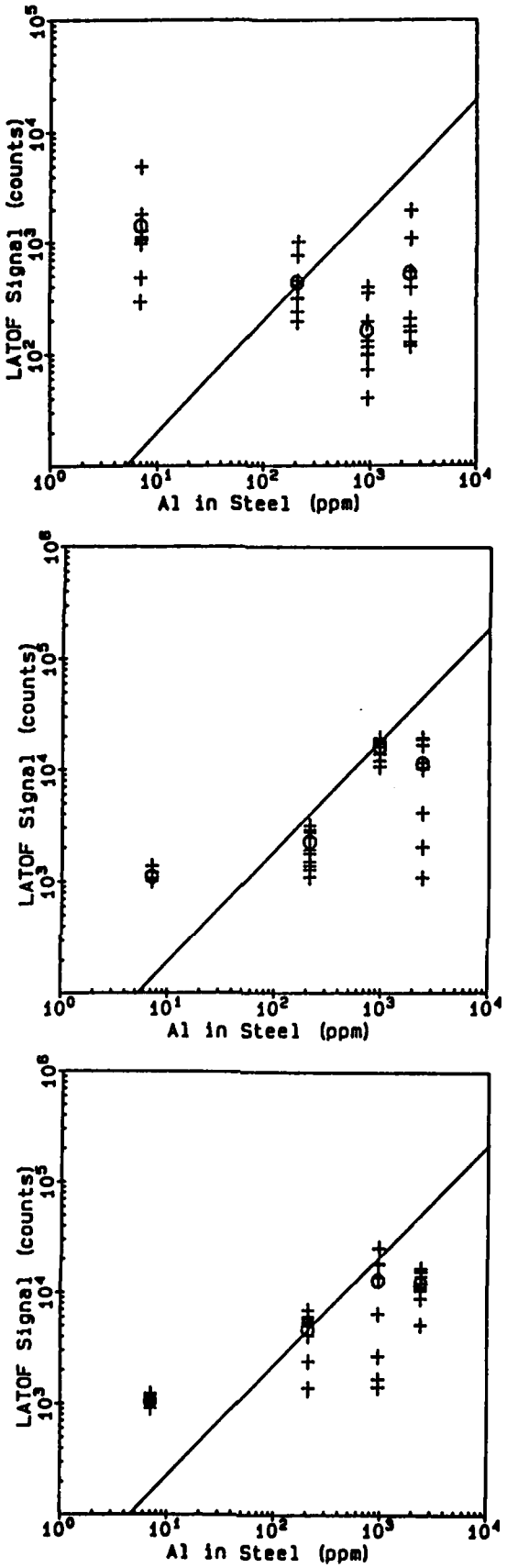

Figure 28. Correlation of Al RIS signal with concentration in NBS steel standards. Data for the top plot was taken before any cleaning, the middle after cleaning with 100 laser shots, and the bottom after an additional 100 shots cleaning. The power density during analysis was 6×10^6, 3×10^7 and 4×10^7 W cm^{-2} (top, middle and bottom plot). The lack of convincing correlation may be due to incomplete ablation of the surface.

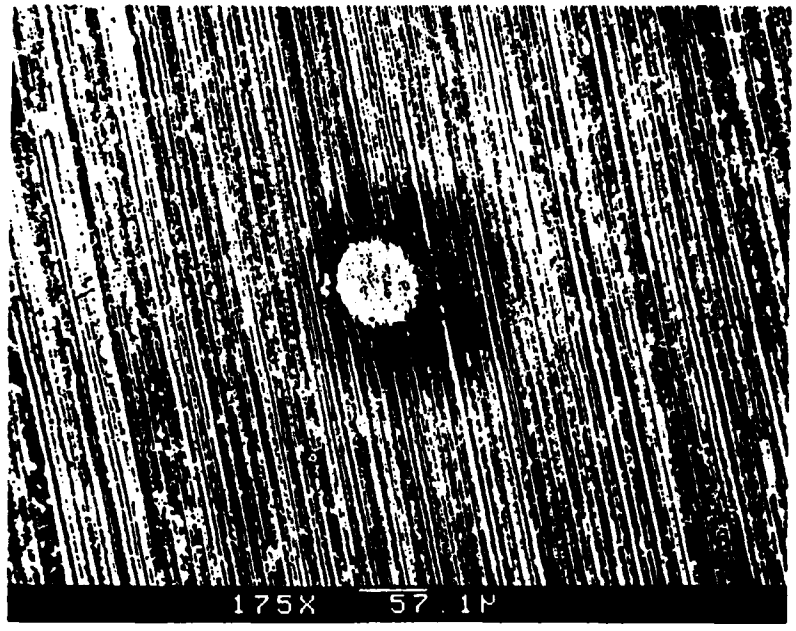

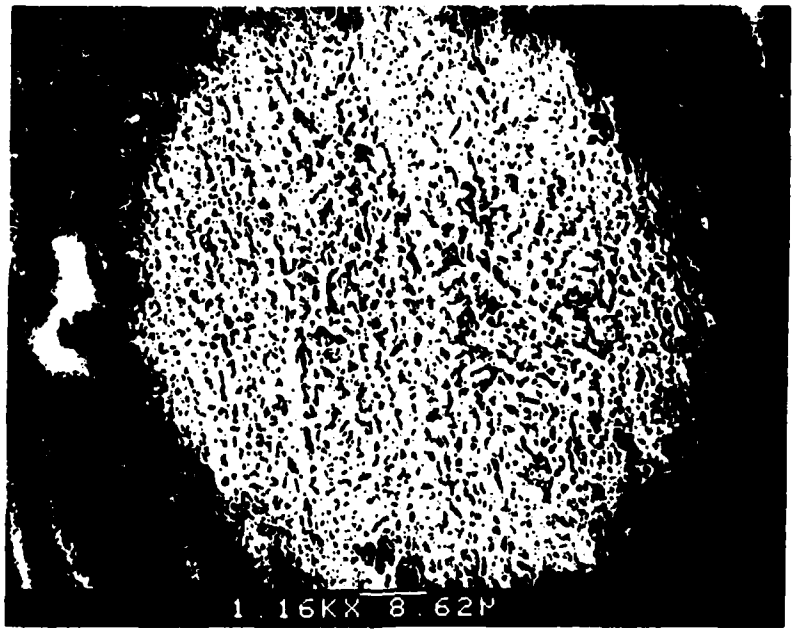

Figure 29. Scanning electron micrograph of the 7 ppm Al in steel sample after analysis (Figure 28, bottom). The mottled surface may be due to partial melting and distillation of the higher vapor pressure Al from the surface.

V. OTHER INFORMATION

1. Publications Resulting From This Effort

"Post-Ablation Resonance Ionization Spectroscopy for Ultra-Trace Element Analysis," N. Thonnard and D.W. Beekman, in preparation (1987).

2. Professional Personnel Associated With Research Effort

N. Thonnard - Principal Investigator
D.W. Beekman - Physicist
M.C. Wright - Physicist
R. Sangsingkeow - Electrical Engineer
B.A. Cameron - Product Engineer

3. Degrees Awarded

None

4. Interactions

Contacts were initiated with Drs. Melvin C. Ohmer (2/19/87) and Patrick M. Hemenger (2/24/87) at the Materials Laboratory of the Air Force Wright Aeronautical Laboratories to determine some of the critical trace analysis needs in the semiconductor and other materials research areas. For metallic impurities in silicon, it would be desirable to detect impurities in the 10^{11} cm^{-3} concentration range (ppt). It would also be desirable to determine O and C concentrations in the low 10^{15} cm^{-3} range. Analysis methods for amorphous silicon are not as well developed, but as the laser ablation/RIS method is independent of the crystalline phase of the sample, the same sensitivities should be achievable. In GaAs, it is desirable to determine Cr, Fe and Si at the 10^{13} to 10^{14} cm^{-3} level, while many of the doping constituents for HgCdTe need to be determined.

Other interests concern non-linear materials, where impurities result in optical absorption. For example Si and C impurities in AgGaSe are critical. Drs. Ohmer and Hemenger indicated they have access to many materials with known impurity levels that they would be able to supply us for test and calibration purposes.

Several meetings and discussions with Dr. Keith Boyer, consultant to the Company and to Los Alamos National Laboratory and the University of Illinois in Chicago, during October and November, 1986, have improved our understanding of the ablation process. He suggested using much shorter wavelengths for the ablation laser to improve atomization of the sample surface. This is especially true for silicon, which does not absorb longer wavelengths effectively.

VI. SUMMARY AND DISCUSSION

During this Phase I feasibility study we demonstrated the analytical sensitivity and selectivity possible for impurity determination in semiconductor materials by combining laser ablation with resonance ionization spectroscopy. Results from specific tasks undertaken follow:

1. Nd:YAG laser characterization for ablation studies. Even though a wide range of pulse-widths could be obtained from the laser with appropriate changes in lamp voltage and Q-switch delay, large pulse-to-pulse output fluctuations limit the useful range to 15 to 45 nsec. For best beam uniformity, the laser should be operated with nominal parameters while output changes are made with external components.

2. Cratering studies in silicon and steel indicated that at high power densities, (10^{11} W cm^{-2}) the ablated crater is much larger in diameter than the ablating laser beam. At power densities of $\sim 5 \times 10^{9}$ W cm^{-2} or less, the affected area on the sample is approximately equivalent to the laser beam diameter. At power densities typical of the RIS studies, ($\sim 5 \times 10^{7}$ W cm^{-2}) no marks were made on the sample, making it difficult to estimate the amount of material removed. At the power densities in which crater profiles could be measured, the volume of the crater was proportional to the number of laser shots. No significant differences could be detected between ablation with 1064 nm or 532 nm radiation, nor could differences be detected between 15 and 45 nsec pulses. The power density threshold for ablation of silicon was definitely less than for steel, while at the same power density, approximately twice as much silicon was ablated per laser shot than steel.

3. A simple RIS-TOF mass spectrometer system utilizing laser ablation for sample volatilization was constructed. The system had sufficient resolution and sensitivity to assess the potential of the analytical method.

4. Analysis of silicon samples containing known concentrations of gallium (0.48 to 58 ppm) indicated very high sensitivity and low background. Because laser ablation is only used to volatilize a representative fraction of the sample, the ablating laser energy is low and few ions are produced. The timing freedom obtainable with independent ionization using RIS allows discrimination against interferences. The overall descrimination in the ionization process is $>10^8$, while a sensitivity of $\sim$15 ppb Ga in Si was shown after only 50 seconds of analysis time. Minor changes in operating mode could easily reduce the detection limit to a part in 10^{10}. The ultimate detection limit could approach a part in 10^{14}.

We recommend that an analysis system capable of detecting impurities in semiconductor materials at the sub-parts per billion level be assembled based on sample volatilization with laser ablation, resonance ionization, and time-of-flight mass spectrometry. From the research completed during this feasibility study and information in the literature, we anticipate the system will have the following features and characteristics:

1. UV ablation wavelength; either fourth harmonic of Nd:YAG (266 nm) or N_2 laser (337 nm).
2. Analysis spot may be as small as 5 micrometers.
3. Sample insertion lock with sample position viewing and manipulation.
4. Sample cleaning provisions; either by laser ablation, ion bombardment or electron bombardment.
5. RIS laser system useable for more than 80 elements of the periodic table without requiring major reconfiguration.
6. Suppression of background ion signals by either pulsing accelerating electrode voltages, energy filtering using reflection type of time-of-flight system, or a combination of both.
7. Data acquisition with a computer-controlled transient digitizer allowing calibration of the data on a shot-by-shot basis.

A system configured as described above would have a detection limit for most elements in the part in 10^{12} range, with perhaps a sensitivity limit of a part in 10^{10} or 10^9 for a dozen elements in the upper right corner of the periodic table. The region analyzed could be as small as 5 μm. This capability would be of significant interest in the semiconductor and materials research fields of the Air Force and the overall scientific and industrial community.

ACKNOWLEDGEMENTS

Many individuals contributed their ideas, experiences and time to this project, for which we wish to acknowledge their support. Special thanks go to Keith Boyer and Hal Schmitt, who helped conceive this program and encouraged us with their strong support. Alex Cameron and Tum Sangsingkeow were invaluable in helping us assemble a TOF system with a minimum of new components, while Jim Parks and Michael Wright made numerous valuable suggestions; their help was much appreciated. We would also like to thank the Submicron Physics Group in the Health and Safety Research Division of Oak Ridge National Laboratory for the use of their scanning electron microscope.

LITERATURE CITED

1. V. S. Ban and B. E. Knox, "Mass Spectrometric Studies of Laser Produced Vapor Species," Int. J. Mass Spectrom. Ion Phys. 3, 524 (1969).

2. R. J. Conzemius and J. M. Capellen, "A Review of the Applications to Solids of the Laser Ion Source in Mass Spectrometry," Int. J. Mass Spectron. Ion Phys., 34, 197 (1980).

3. G. S. Hurst, M. G. Payne, M. H. Nayfeh, J. P. Judish and E. B. Wagner, "Saturated Two-Photon Resonance Ionization of He (2^1S)," Phys. Rev. Lett. 35, 82 (1975).

4. M. G. Payne, G. S. Hurst, M. H. Nayfeh, J. P. Judish, C. H. Chen, E. B. Wagner and J. P. Young, "Kinetics of He (2^1S) Using Resonance Ionization Spectroscopy," Phys. Rev. Lett. 35, 1154 (1975).

5. G. S. Hurst, M. G. Payne, S. D. Kramer and J. P. Young, "Resonance Ionization Spectroscopy and One Atom Detection," Rev. Mod. Phys. 51, 767 (1979).

6. J. E. Parks, H. W. Schmitt, G. S. Hurst, and W. M. Fairbank, Jr., "Sputter-Initiated Resonance Ionization Spectroscopy," Thin Solid Films 108, 69 (1983).

7. J. E. Parks, H. W. Schmitt, G. S. Hurst, and W. M. Fairbank, Jr., "Sputter Initiated RIS (SIRIS) for Analysis of Semiconductor Impurities," Inst. Phys. Conf. Ser. No. 71, 167 (1984).

8. D. W. Beekman, T. A. Callcott, S. D. Kramer, E. T. Arakawa, G. S. Hurst, E. Nussbaum, "Resonance Ionization Source For Mass Spectroscopy," Int. J. Mass Sepctrom. Ion Phys. 34, 89 (1980).

9. S. Mayo, T. B. Lucatorto, and G. G. Luther, "Laser Ablation and Resonance Ionization Spectrometry for Trace Analysis of Solids," Anal. Chem. 54, 553 (1982).

10. D. W. Beekman and T. A. Callcott, "Laser Ablation Studies Using RIS," Inst. Phys. Conf. Ser. No. 71, 143 (1984).

11. K. Boyer, private communication (1986).

12. L. J. Moore, private communication (1985).

13. W. C. Wiley and I. H. McLaren, "Time-of-Flight Mass Spectrometer With Improved Resolution," Rev. Sci. Instr. 26, 1150 (1955).

END

8-87

DTIC